Geochemistry Geophysics Geosystems G3
AN ELECTRONIC JOURNAL OF THE EARTH SCIENCES
Published by AGU and the Geochemical Society

Article
Volume 6, Number 7
19 July 2005
Q07006, doi:10.1029/2004GC000895
ISSN: 1525-2027

Geochemical mapping of the Mariana arc-basin system: Implications for the nature and distribution of subduction components

Julian A. Pearce
School of Earth, Ocean and Planetary Sciences, Cardiff University, Park Place, Cardiff CF10 3YE, UK (pearceja@cardiff.ac.uk)

Robert J. Stern
Geosciences Department, University of Texas at Dallas, Richardson, Texas 75083-0688, USA

Sherman H. Bloomer
College of Science, Oregon State University, Corvallis, Oregon 97331, USA

Patty Fryer
Hawaii Institute of Geophysics and Planetology, 2525 Correa Road, Honolulu, Hawaii 96822, USA

[1] A new ICP-MS database for glasses from the Mariana Trough, together with published and new ICP-MS data from the Mariana arc, provides the basis for geochemical mapping of the Mariana arc-basin system. The geochemical maps presented here are based on the graphic representation of spatial variations in geochemical proxies for the principal mantle and subduction components. The focus is on three elements with high and similar partition coefficients but different behavior in subduction systems, namely, Ba, Th, and Nb. Two elements with different partition coefficients, Ta and Yb, are used as normalizing factors. Ratio maps (Ta/Yb, Nb/Ta, Th/Ta, Ba/Ta, Ba/Th) provide the simplest petrogenetic insights, subduction zone addition maps based on deviations from a MORB array provide more quantitative insights, and component maps represent an attempt to isolate the different subduction components. The maps shown here indicate the presence of a variably depleted asthenosphere and three added components: a Nb-Th-Ba component, a Th-Ba deep-subduction component, and a Ba-only shallow-subduction component. The asthenosphere entering the system is enriched relative to N-MORB and appears to be focused at three sites within the Mariana Trough. The Nb-Th-Ba component is present mainly in the north of the arc (the Northern Seamount province and northern Central Island Province), the northern edge of the Mariana Trough, and two locations within the Southern Seamount Province. It has a distinctively high Nb/Ta ratio and a moderate enrichment in Th and Ba relative to Nb. Its composition and distribution indicate that it may not be part of the present subduction system but instead originates in mantle lithosphere previously enriched above the subduction zone by addition of small-degree, subduction-modified mantle melts. The Th-Ba component is present throughout the arc and, in minor amounts, in parts of the back-arc basin. The Ba-only component is mainly present in the central part of the arc and at the edges of the back-arc basin. Overall, the geochemical maps provide a new perspective on the geochemical processes that accompany the evolution of an arc basin system from prerifting lithospheric enrichment, through arc-rifting to arc volcanism and back-arc spreading.

Components: 21,288 words, 12 figures, 5 tables.

Keywords: Mariana arc; Mariana Trough; subduction; trace elements; geochemical mapping; arc rifting.

Index Terms: 1020 Geochemistry: Composition of the continental crust; 1065 Geochemistry: Major and trace element geochemistry; 8120 Tectonophysics: Dynamics of lithosphere and mantle: general (1213)

Received 8 December 2004; **Revised** 4 April 2005; **Accepted** 25 April 2005; **Published** 19 July 2005.

Pearce, J. A., R. J. Stern, S. H. Bloomer, and P. Fryer (2005), Geochemical mapping of the Mariana arc-basin system: Implications for the nature and distribution of subduction components, *Geochem. Geophys. Geosyst.*, *6*, Q07006, doi:10.1029/2004GC000895.

1. Introduction

[2] Geochemical mapping has many applied applications, and geochemical maps have proven valuable for agriculture, mining and industrial health. They are rarely used for "pure" scientific purposes. However, they do have an underestimated function in petrogenetic interpretations, by enabling chosen geochemical parameters to be studied in a spatial context. Potentially, they can then be used to study mantle domains, mantle flow and the distribution of mantle source components. The aim of this paper is to apply geochemical mapping to the interpretation of the Mariana arc-basin system.

[3] *Stern et al.* [2003] reviewed the geochemical and geodynamic characteristics of the Mariana arc and Mariana Trough back-arc basin as part of the greater Izu-Bonin-Mariana system and highlighted its significance for investigating arc rifting and the early evolution of back-arc spreading. To provide a geochemical mapping contribution to this investigation, we have assembled a new ICP-MS geochemical database of lavas from the Mariana Trough and Southern Mariana arc. This database, coupled with published data from the Central and Northern Mariana arc, gives the geographic and geochemical coverage required for this work.

2. Tectonic Subdivisions of the Mariana Arc-Basin System

[4] The Mariana arc-basin magmatic system (Figure 1) is made up of two parts: the Mariana arc; and the Mariana Trough. The Mariana arc has a classic arcuate geometry and is made up of some 40 active submarine and subaerial volcanoes. The Mariana Trough is an actively extending back-arc basin which converges on the arc in the north and south, and reaches a maximum distance of about 100 km behind the arc in its center. Both can usefully be subdivided into South, Central and Northern sections, as also illustrated in Table 1.

2.1. Mariana Arc

[5] The Southern Seamount Province (SSP), south of 16°N, comprises nine submarine volcanic edifices, four of which (Ruby, Diamante, Esmeralda, Tracey) are named, the others unnamed [*Dixon and Stern*, 1983; *Stern et al.*, 1989]. It is constructed on back-arc crust west of the fore-arc frontal ridge containing the islands of Guam, Rota, Saipan and Tinian. The Mariana Trough to the west is actively spreading. In the extreme south, the arc bends to run parallel with the trench and eventually converges with the remnant arc of the Mariana Ridge [*Fryer et al.*, 1998; *Martinez et al.*, 2000].

[6] The Central Island Province (CIP), from 16° to 20.7°N, is dominated by nine subaerial volcanoes from Uracas in the north to Anatahan in the south [e.g., *Woodhead*, 1989; *Elliott et al.*, 1997], although it also includes a number of volcanic seamounts [*Bloomer et al.*, 1989a]. It was constructed on rifted and spread back-arc basin lithosphere. As with the SSP, the Mariana Trough to the west is actively spreading.

[7] The Northern Seamount Province (NSP), from 20.7° to 24°N, is a continuation of the CIP. Unlike the CIP, however, all its volcanoes are submarine and the Mariana Trough to its rear lacks a clear spreading axis. It appears to be constructed on preexisting arc crust rather than oceanic crust. Its southern part, from 20.7° to 23°N, is labeled the Southern NSP (S-NSP). This province also has chains of small volcanoes extending into the Mariana Trough along WSW to SSW trends [*Hussong and Fryer*, 1983; *Stern et al.*, 1993; *Fryer et al.*, 1997], although a lack of necessary data excludes them from this study. Its northern part, from 23° to 24°N, is termed the Northern NSP (N-NSP) and marks the part of the system where the Mariana Trough and Mariana arc meet in a zone of arc rifting about 150 km long [e.g., *Gribble et al.*, 1998]. This is also a region where convergence between the Pacific and Philippine Sea plates is highly oblique, with implications for the PTt path, and hence fluid-release history, of the subducting plate. Many of the rocks in this part of the arc have shoshonitic compositions [*Bloomer et al.*, 1989b; *Lin et al.*, 1989] and thus it has been also been termed the "Alkalic Volcano Province" [*Sun and Stern*, 2001].

2.2. Mariana Trough

[8] The Southern Mariana Trough (SMT), from 12.5°N to 17.5°N, varies considerably in morphol-

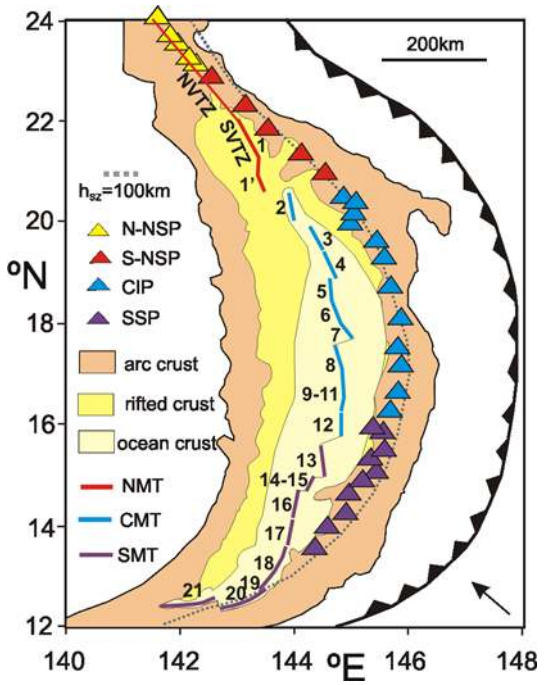

Figure 1. Map of the Mariana arc-basin system showing the arc, rifted crust, and new oceanic crust. The map also shows the various subdivisions of the arc and the segments within the Mariana Trough as identified in Table 1. Abbreviations: NSP, Northern Seamount Province; CIP, Central Island Province; SSP, Southern Seamount Province; VTZ, Volcano-Tectonic Zone; MT, Mariana Trough; N, North; S, South; C, Central.

ogy along its length. South of about 14.1°N, it has an inflated (fast spreading) morphology, forming a shallow (<3 km) platform [*Fryer*, 1995] which converges on, and intersects, the Southern Seamount Province of the Mariana Arc at about 12.5°N. This is consistent with recent GPS results indicating faster spreading in the south than in the north [*Kato et al.*, 2003]. North of 14.1°N, the ridge attains the morphology of a typical slow-spreading ridge which is initially deep, but becomes shallower north of 15°N. *Stüben et al.* [1998] have subdivided this part of the ridge into a number of segments, as depicted in Figure 1. We have taken the northern boundary of this part of the Mariana Trough as the Pagan Fracture Zone at about 17.5°N [*Gribble et al.*, 1996].

[9] The Central Mariana Trough (CMT), from 17.6°N to 21°N, includes the well-studied part from the Pagan FZ from about 17.6°N to about 18.5°N [*Hawkins et al.*, 1990; *Volpe et al.*, 1987]. The ridge to the north, from 18.5° to 20.5°N, includes segments 2-4 of *Yamazaki et al.* [2003]. At its northern end, it converges on, but does not intersect, the northern part of the Central Island Province of the Mariana arc. We have taken the northern boundary of this part of the Mariana Trough as the northernmost extent of true spreading, although we note that its location is still debated. *Martinez et al.* [2000] have the boundary at about 19.7°N, with an amagmatic central graben and then a rift axis to the north. *Yamazaki et al.* [2003] have the boundary at 22.1°N. For this paper, we choose a boundary at about 21°N between segments 1 and 1′ of *Yamazaki et al.* [2003], and between the eastern and western limbs of the Central Graben of *Martinez et al.* [2000]; this is based on the fact that Segment 1′ has geochemical characteristics of the spreading Mariana Trough to the south, whereas Segment 1 has characteristics of the rifting or diffuse spreading Mariana Trough to the north (see Tables 2 and 3).

[10] The Northern Mariana Trough (NMT), from 21°N to 24°N, may be subdivided into three parts. The Southern Volcano-Tectonic Zone (SVTZ), from 21° to 22°N, converges on the S-NSP part of the arc at the latitude of Fukujin Seamount. It is thus equivalent to Segment 1 of *Yamazaki et al.* [2003]. It is dominated by fissure eruptions associated with a relatively shallow (<2800 m), ridge-like feature. The Northern Volcano-Tectonic Zone (NVTZ), 22° to 23°N, is dominated by volcanic edifices separated by rift basins. It runs subparallel to where the arc would lie but there is no actual arc activity at these latitudes, indicating that the NVTZ may have "captured" both the arc and back-arc magmatism [*Gribble et al.*, 1998; *Stern et al.*, 2003]. The third part, not sampled, comprises the small rifted basins within the N-NSP.

3. Geochemical Database

[11] This paper utilizes our new ICP-MS data set for samples from the Mariana Trough. Many of the samples already had major element, XRF and INAA (or isotope dilution) trace element data and the new data adds information on certain petrogenetically important elements, especially, Nb, Ta, Hf, Th, and U, as well as providing complete REE coverage. The Mariana Trough samples used were dredged from 20–23°N [*Stern et al.*, 1990; *Gribble et al.*, 1998], 15–17°N [*Gribble et al.*, 1996], 13–15°N (R/V *Melville Cook 7* cruise: previously unpublished) and 12.5–13°N (Cook 6 cruise and Jason-42 dives: previously unpublished). The only suite of samples we did not analyze is the Alvin sample set from 17–19°N for which *Hawkins et al.*

Table 1. Simplified Subdivision of the Mariana Trough and Mariana Arc for the Purpose of Grouping Samples for Geochemical Plots[a]

Trough Province	Segment	Latitude (Start)	Latitude (End)	Arc Province	Volcano	Latitude
NMT(N)	Intraarc rift	24.0N	23.1N	NNSP	Fukutoku	23.6N
				NNSP	Hiyoshi volcanoes	23.2–23.4N
NMT(C)	NVTZ	23.1N	22.1N	SNSP	Nikko	23.1N
				SNSP	Ichiyo	23.0N
				SNSP	Fukuyama	22.4N
NMT(S)	SVTZ	22.1N	21.0N	SNSP	Fukujin	21.9N
				SNSP	Eifuku	21.4N
				SNSP	Daikoku	21.3N
				SNSP	S. Daikoku.	21.0N
CMT(N)	1	21.0N	20.5N	CIP	NW Urucas	21.0N
				CIP	Uracas	20.5N
CMT(N)	2	20.5N	20.0N	CIP	Ahyi	20.4N
				CIP	Maug	20.0N
CMT(N)	3	19.9N	19.4N	CIP	Asuncion	19.7N
CMT(N)	4	19.4N	18.9N	CIP	Cheref	19.4N
CMT(C)	5	18.9N	18.5N	CIP	Agrigan	18.8N
CMT(C)	6	18.5N	17.9N	CIP	Pagan	18.1N
CMT(C)	7	17.9N	17.7N			
	Pagan FZ	17.7N	17.5N	CIP	Alamagan	17.6N
CMT(S)	8	17.5N	16.9N	CIP	Guguan	17.3N
CMT(S)	9	16.9N	16.7N	CIP	Saragan	16.7N
CMT(S)	10	16.7N.	16.6N			
CMT(S)	11	16.6N	16.4N	CIP	Anatahan	16.4N
CMT(S)	12	16.4N	15.7N	SSP	Diamante	15.9N
	FZ	15.7N	15.6N	SSP	Ruby	15.6N
SMT(N)	13	15.5N	15.1N	SSP	N. Esmeralda	15.4N
SMT(N)	14	15.1N	14.9N	SSP	Esmeralda	15.0N
SMT(N)	15	14.9N	14.8N			
SMT(N)	16	14.8N	14.2N	SSP	unnamed	14.6N
				SSP	unnamed	14.3N
SMT(C)	17	14.2N	13.7N	SSP	unnamed	14.0N
SMT(C)	18	13.7N	12.8N	SSP	Tracey	13.6N
				SSP	unnamed	13.5N
SMT(S)	19	12.8N	12.7N			
SMT(S)	20	12.7N	12.2N			
SMT(S)	21	12.3N	12.2N			

[a] The Mariana Trough is divided into Northern (NMT), Central (CMT), and Southern (SMT) parts, each in turn having northern (N), central (C), and southern (S) subgroups. Note that the precise boundary between the NMT and CMT is still debated, and that between the CMT and SMT is for convenience of geochemical grouping and differs from the boundary based on slow-to-fast ridge morphology, which lies between SMT(N) and SMT(C). The Northern (nonspreading) part of the Mariana Trough is divided into rift, Northern Volcanic Tectonic Zone (NVTZ), and Southern Volcanic Tectonic Zone (SVTZ) segments according to *Martinez et al.* [1995]. The Central and Southern parts are divided into 21 ridge segments based on surveys of *Hawkins et al.* [1990], *Martinez Et Al.* [2000], and *Yamazaki et al.* [2003]. The arc is divided into a Northern Seamount Province (NSP) with Northern (N-NSP) and Southern (S-NSP) parts, a Central Island Province (CIP), and a Southern Seamount Province (SSP) according to *Stern et al.* [1988]. The arc volcanoes listed are those included in this study. Sample numbers for each segment can be obtained from the HTML version of Table 3, though note that the segment 6 data set also includes published data of Hawkins and coworkers.

[1990] and *Volpe et al.* [1987] have published some complete analyses. However, we did analyze some representative glasses from 18° 09′N [*Ikeda et al.*, 1998]. The complete data set (major element data from the publications listed above plus the new ICPMS data) is presented in Table 3.

[12] For the arc, the data used are those of *Bloomer et al.* [1989b], *Peate and Pearce* [1998], and *Sun and Stern* [2001] for the NSP and the seamounts of the CIP. Data from the subaerial volcanoes of the CIP are taken from *Woodhead* [1989], *Woodhead et al.* [2001], and *Elliott et al.* [1997]. New ICP-MS analyses were also carried out for the Southern Seamount Province, extending the data sets published by *Dixon and Stern* [1983], *Stern and Bibee* [1984], and *Stern et al.* [1989]. All new analyses were carried out by ICP-MS using the Thermo-elemental X-series machine at Cardiff and the dissolution method described by *Pearce et al.* [1995]. Accuracies (with respect to international standards JB1 and BIR-1) and relative standard deviations obtained from multiple dissolutions are given in Table 3.

Table 2. Average Analyses for Lavas From the Various Parts of the Mariana Subduction System as Depicted in Table 1[a]

Location	SMT	SMT	SMT	CMT	CMT	CMT	NMT	NMT				
Segment	21-19	18-17	16-13	12-8	7-5	4-1′	SVTZ	NVTZ	SSP	CIP	SNSP	NNSP
SiO_2	55.61	51.88	50.90	50.96	51.25	51.45	52.10	52.03	51.57	53.14	54.94	51.38
TiO_2	1.43	1.49	1.61	1.09	1.27	1.22	0.99	0.98	0.80	0.77	0.80	0.85
Al_2O_3	15.11	15.63	15.84	16.96	16.64	16.91	16.27	17.71	16.45	17.76	16.98	18.54
Fe_2O_3*	10.45	10.48	10.26	8.77	8.35	8.71	8.73	10.73	8.75	9.90	9.71	9.57
MgO	3.64	5.85	6.58	6.86	7.20	7.25	6.14	4.55	6.11	4.84	4.51	4.46
MnO	0.20	0.19	0.18	0.14	0.16	0.16	0.15	0.18	0.18	0.19	0.18	0.20
CaO	7.65	10.42	11.04	11.50	11.06	11.17	11.01	10.66	11.07	9.92	8.76	9.43
Na_2O	3.73	3.10	3.39	2.73	3.05	2.98	2.69	2.66	2.47	2.65	2.87	3.09
K_2O	0.71	0.14	0.21	0.33	0.33	0.30	0.44	0.48	0.73	0.71	1.10	2.16
P_2O_5	0.24	0.18	0.17	0.15	0.14	0.16	0.15	0.14	0.15	0.13	0.16	0.33
Total	98.77	99.36	100.20	99.49	99.44	100.31	98.68	100.11	98.27	100.01	100.01	100.01
Sc	34.4	34.7	36.0	32.8	34.5	34.3	35.5	40.1	38.9	36.7	33.3	24.0
V	332	276	277	234	231	240	249	350	295	256	245	244
Cr	24	177	251	243	271	258	215	98	164	53	59	46
Co	31.1	35.3	38.6	35.8	34.2	38.1	35.0	36.6	38.7	29.7	28.4	27.0
Ni	31	95	122	98	103	157	101	55	57	24	31	18
Cu	95	63	64	69	63	66	71	108	109	88	106	127
Ga	22.3	16.0	17.6	15.0	15.5	15.7	14.6	16.6	15.7	15.9	16.1	18.3
Rb	14.2	2.3	2.5	5.0	4.1	5.0	7.3	8.7	12.4	12.6	21.7	59.1
Sr	400	152	171	220	200	223	281	337	336	306	437	791
Y	39.7	31.6	38.0	24.3	28.1	28.5	22.0	21.8	21.5	22.9	24.3	24.6
Zr	147.8	96.9	134.9	73.2	93.3	93.2	71.5	60.9	55.4	64.5	78.4	138.9
Nb	4.37	1.78	4.51	3.21	3.28	4.29	2.90	2.32	1.37	1.24	2.48	7.26
Cs	0.25	0.04	0.03	0.09	0.05	0.07	0.14	0.21	0.32	0.40	0.51	0.71
Ba	188	27	25	57	37	49	123	155	167	203	389	765
La	14.15	3.78	5.47	4.60	5.59	5.79	7.23	8.13	6.28	5.68	14.29	42.57
Ce	31.73	11.13	15.59	11.40	13.92	14.22	15.56	17.02	13.59	12.92	28.56	80.45
Pr	4.15	1.97	2.63	1.79	2.23	2.15	2.25	2.22	2.13	2.06	3.60	8.25
Nd	19.00	10.17	13.41	8.79	10.95	10.41	10.37	10.75	9.97	9.12	15.79	36.02
Sm	5.47	3.31	4.25	2.73	3.25	3.25	2.84	2.90	2.77	2.61	3.72	6.69
Eu	1.79	1.20	1.47	1.00	1.17	1.17	1.03	1.04	0.98	0.93	1.19	1.90
Gd	5.87	4.21	5.19	3.33	3.99	4.11	3.33	3.25	3.19	3.26	3.96	5.62
Tb	1.00	0.75	0.93	0.60	0.68	0.72	0.57	0.56	0.53	0.63	0.62	0.72
Dy	6.35	5.04	6.11	3.89	4.43	4.56	3.59	3.50	3.40	3.62	4.06	4.64
Ho	1.34	1.08	1.30	0.82	0.94	0.97	0.76	0.74	0.73	0.81	0.80	0.83
Er	3.90	3.10	3.70	2.36	2.67	2.78	2.15	2.14	2.07	2.25	2.45	2.55
Tm	0.61	0.49	0.57	0.36	0.42	0.43	0.34	0.33	0.33	0.36	0.35	0.33
Yb	3.84	3.09	3.61	2.31	2.60	2.69	2.12	2.11	2.10	2.22	2.41	0.45
Lu	0.61	0.48	0.56	0.36	0.40	0.42	0.33	0.34	0.33	0.37	0.36	0.35
Hf	3.76	2.46	3.24	1.87	2.28	2.28	1.82	1.61	1.57	1.80	2.03	3.09
Ta	0.257	0.133	0.304	0.214	0.220	0.279	0.175	0.134	0.083	0.084	0.122	0.335
Pb	3.27	0.75	1.04	0.83	0.50	0.81	1.75	2.27	1.74	2.57	4.12	7.61
Th	1.388	0.214	0.317	0.446	0.424	0.548	0.848	1.080	0.722	0.803	2.328	7.738
U	0.504	0.103	0.149	0.148	0.159	0.181	0.257	0.383	0.360	0.335	0.762	2.158

[a] The full set of new ICP-MS analyses is given in the HTML version of Table 3. Note that the SMT(16-13) average is close to the composition of Mariana Trough MORB. Abbreviations are as in Table 1.

[13] Because the absolute concentrations of Nb and Ta, and the Nb/Ta ratio, play an important part in this study, all the samples in Table 3 were analyzed a second time for a small subset of elements (Zr, Nb, Yb, Hf, Ta, Th) and with long time-integrated dwell-times. Calibration for Nb and Ta is based on the BHVO-1, BCR-1, W-2 and AGV-1 values of *Eggins et al.* [1997] with BIR-1 analyzed as an unknown as a check of low concentrations. Importantly, the detection limit for the key element, Ta, is <0.001 ppm, i.e., well below its concentration in even the most depleted sample analyzed. The values quoted for these elements in Table 2 are weighted averages of the two analyses. The NSP and CIP samples of *Peate and Pearce* [1998] (some of which were also analyzed by *Sun and Stern* [2001]) and the CIP samples of *Woodhead et al.* [2001] were also reanalyzed for these elements to provide a consistent data set. In fact, only the Ta required amending and, even then, differences with the original values are

Table 3 (Representative Sample). Complete Database of New ICP-MS Analyses for the Mariana Trough[a] [The full Table 3 is available in the HTML version of this article at http://www.g-cubed.org.]

Sample	Cook 6-5-1	Cook 6-5-4	Cook 6-5-6	Cook 6-6-2	Cook 6-6-3	Cook 6-6-4	Cook 6-6-5	Cook 6-6-7	J42-1	J42-3	J42-4	J42-5	J42-9	J42-10
Longitude	142.03	142.03	142.03	142.27	142.27	142.27	142.27	142.27	143.61	143.62	143.62	143.61	143.62	143.62
Latitude	12.43	12.43	12.43	12.44	12.44	12.44	12.44	12.44	12.93	12.95	12.95	12.95	12.96	12.96
Segment	21	21	21	21	21	21	21	21	19	19	19	19	19	19
Depth, m	2466	2466	2466	1875	1875	1875	1875	1875	2880	2871	2835	2803	2875	2893
SiO_2	55.29	55.35	55.55	54.02	55.66	54.30	56.35	54.01	57.20	54.99	55.72	58.81	55.50	55.74
TiO_2	1.11	1.10	1.10	1.13	1.25	1.16	1.36	1.16	1.79	1.84	1.85	1.43	1.95	1.48
Al_2O_3	15.59	15.36	15.51	15.70	15.39	15.69	15.25	15.64	14.24	14.59	14.25	15.51	13.98	15.14
FeO*	9.41	9.65	9.43	9.65	9.56	9.64	9.30	9.46	11.30	12.58	12.41	9.06	12.53	11.26
MgO	3.96	4.03	3.98	4.85	3.96	4.75	3.51	4.72	2.64	3.26	3.22	2.24	2.98	3.31
MnO	0.19	0.17	0.18	0.20	0.18	0.18	0.17	0.21	0.21	0.25	0.22	0.21	0.21	0.18
CaO	8.06	8.21	8.13	9.01	7.97	9.01	7.33	9.10	6.31	7.26	7.05	5.80	6.97	7.51
Na_2O	3.25	3.23	3.32	3.71	4.03	3.71	4.22	3.73	4.01	3.55	3.76	4.49	3.80	3.44
K_2O	1.21	1.23	1.19	0.79	1.02	0.80	1.06	0.75	0.40	0.33	0.40	0.45	0.40	0.37
P_2O_5	0.28	0.27	0.28	0.25	0.26	0.25	0.28	0.24	0.25	0.19	0.19	0.28	0.21	0.19
Total	98.35	98.60	98.67	99.31	99.28	99.49	98.83	99.02	98.35	98.84	99.07	98.28	98.53	98.62
Sc	33.1	34.1	37.0	37.4	29.6	37.0	27.2	30.3	42.8	34.1	38.0	26.7	36.8	37.2
V	342	355	387	331	304	309	286	274	369	377	413	115	417	357
Cr	58	21	20	46	14	77	35	33	15	11	4	5	6	13
Co	30	32	33	35	28	33	25	29	37	31	37	16	37	33
Ni	37	42	18	32	20	30	17	21	60	41	34	27	41	31
Cu	157	163	175	141	140	126	133	117	31	44	41	17	47	50
Ga	20.4	21.4	23.4	22.1	20.9	20.2	20.3	18.3	29.7	20.7	24.2	24.3	23.5	22.0
Rb	24.6	25.6	27.6	16.0	19.3	14.7	19.9	13.5	9.9	5.0	7.4	8.5	7.1	7.7
Sr	680	729	802	551	500	498	463	455	228	161	184	211	179	176
Y	25.2	25.9	28.1	28.2	28.0	25.9	27.8	23.4	72.1	43.3	53.6	64.5	51.8	46.9
Zr	111.5	114.1	124.4	121.6	131.2	111.4	135.0	100.6	230.8	138.9	178.2	223.2	174.8	151.3
Nb	3.74	3.89	4.17	3.83	4.32	3.51	4.45	3.19	6.35	3.84	4.67	6.06	4.51	4.31
Cs	0.34	0.36	0.37	0.27	0.33	0.24	0.32	0.22	0.24	0.14	0.17	0.22	0.16	0.21
Ba	378	393	424	227	254	203	254	185	88	52	67	103	64	73
La	24.94	26.17	28.08	15.44	16.99	14.19	16.75	13.02	10.45	5.93	7.97	10.42	7.72	7.05
Ce	49.55	51.80	55.81	33.27	35.80	30.72	35.61	28.10	28.43	16.54	21.79	28.03	21.35	19.00
Pr	5.88	6.12	6.58	4.22	4.46	3.88	4.38	3.53	4.31	2.55	3.28	4.16	3.16	2.79
Nd	24.18	25.22	27.20	18.59	19.34	17.15	18.91	15.65	21.93	13.10	16.76	21.07	16.18	14.19
Sm	5.57	5.79	6.23	4.88	4.94	4.51	4.78	4.09	7.58	4.66	5.80	7.13	5.69	4.97
Eu	1.70	1.78	1.91	1.60	1.59	1.49	1.53	1.34	2.52	1.60	1.96	2.37	1.89	1.69
Gd	4.92	5.16	5.56	4.80	4.80	4.46	4.70	4.03	9.08	5.71	7.04	8.42	6.76	6.04

[a] SVTZ, Southern Volcano-Tectonic Zone(= Segment 1); NVTZ, Northern Volcano-Tectonic Zone; SSP, Southern Seamount Province; Unn, unnamed; Esm, Esmeralda; SSP, Southern Seamount Province; Diam = Diamante. Missing data result from WC contamination; remainder of samples are agate-crushed. Values (in ppm) for JB1 and BIR-1 international standards. RSD, relative standard deviation. Note that RSD values are for multiple separate dissolutions: within-run and single dissolution RSD values are significantly lower. Note also that the deviations from "recommended values" between our Nb and Ta values in JB-1 and Ta in BIR-1 likely reflect inaccurate standard values or values that apply to a different powder batch. Our BIR-1 Ta values are within error of more recent determinations such as those of *Eggins et al.* [1997].

small, as will be seen in Table 5. The *Woodhead et al.* [2001] CIP data are similarly close to published values and will be published separately with new Hf isotope data (J. D. Woodhead et al., manuscript in preparation, 2005).

[14] Given that most of the geochemical features of the arc-basin system have already been discussed in some detail (see the review by *Stern et al.* [2003]), the focus of this paper is on the new data, especially the highly incompatible elements, Ba, Th and Nb. This is an important combination of elements, as all are highly incompatible, with very similar behavior during melting and fractional crystallization. However, they are decoupled by subduction processes. Although the details vary according to the precise residual mineral assemblage present, experiments essentially show that Ba, but not Th, is significantly partitioned into aqueous fluids derived from the subduction zone, while both Ba and Th are significantly partitioned into siliceous melts [e.g., *Keppler*, 1996; *Johnson and Plank*, 1999], results which are supported by empirical studies of subduction-zone metamorphic complexes [e.g., *Sorensen and Grossman*, 1989; *Breeding et al.*, 2004]. In contrast, Nb is probably mobilized from a rutile-bearing slab only in melts at the highest temperatures [e.g., *Ryerson and Watson*, 1987; *Ayers and Watson*, 1993; *Brenan et al.*, 1994]. Ta and Yb are used to normalize these three elements for reasons detailed in the next section. Most other elements are not discussed here through lack of space, but we publish the full database to allow the reader to evaluate other potential geochemical proxies that are not developed here through lack of space.

4. Geochemical Mapping Using Element Ratios

4.1. Use of Trace Element Ratios as Proxies for Subduction and Mantle Processes

[15] Individual incompatible elements have limited use in geochemical mapping because their abundances are modified by partial melting, fractional crystallization and crystal cumulation, as well as mantle composition. Correcting all samples to a given concentration of MgO is difficult to accomplish confidently for arc lavas, which are characteristically evolved, multiply saturated, and rich in phenocrysts. We deal with fractionation and phenocryst accumulation by dividing each element by a trace element that is incompatible and highly conservative in subduction systems. Yb is particularly suitable as it is strongly compatible with eclogitic assemblages and so is one of the most subduction-immobile incompatible elements. It can vary significantly during partial melting, but not in most oceanic subduction systems where the shallow depth and high degree of melting rarely result in residual garnet. The effects of Yb normalization can be seen in Figures 2a and 2b. The geochemical patterns are relocated at Yb = 1 and the normalization reduces inter-pattern variability. Thus a single element such as Nb will be plotted as Nb/Yb. Normalizing to Ta concentrations is potentially even more useful, as Ta is only slightly less incompatible than Ba, Th and Nb. However, it will emerge that there is at least one situation in which Ta is concentrated in a mantle enrichment component, so Yb remains the most reliable normalizing element.

[16] The geochemical pattern in Figure 2c highlights some of the element ratios that can usefully act as proxies for subduction processes and hence form the basis of geochemical maps. There are three principal types of proxy. Ratios of conservative elements with different compatibilities (e.g., Nb/Ta, Nb/Yb) highlight mantle source variations and degree of melting. Ratios of elements of similar incompatibilities, one subduction-mobile and one subduction-immobile, highlight subduction inputs. The most useful of these include Ba/Ta and Th/Ta (or Ba/Nb and Th/Nb), as explained by *Elliott et al.* [1997] in their study of the CIP. As noted earlier, Ba enrichment, and hence high Ba/Ta, characterizes the total subduction component as Ba is released over a wide range of subduction temperatures; in contrast, Th enrichment, and hence high Th/Ta, characterizes only the higher-temperature melt component. In consequence, high Ba/Th characterizes the lower-temperature fluid component because both elements are mobilized in melts but only Ba is mobilized in fluids. The caveat to the use of these proxies is that many of the details of fluid-solid partitioning are poorly understood. However, as will be seen, they appear to give useful first-order information, especially when considering a single subduction system.

4.2. Mapping the Mariana Arc-Basin System Using Trace Element Ratios

[17] Figure 3 gives some maps based on some of the more important element ratios. Each data point is represented by a circle. In Figure 3, we have color-coded the data for black-and-white compatibility on a scale from dark red (high) to pale pink

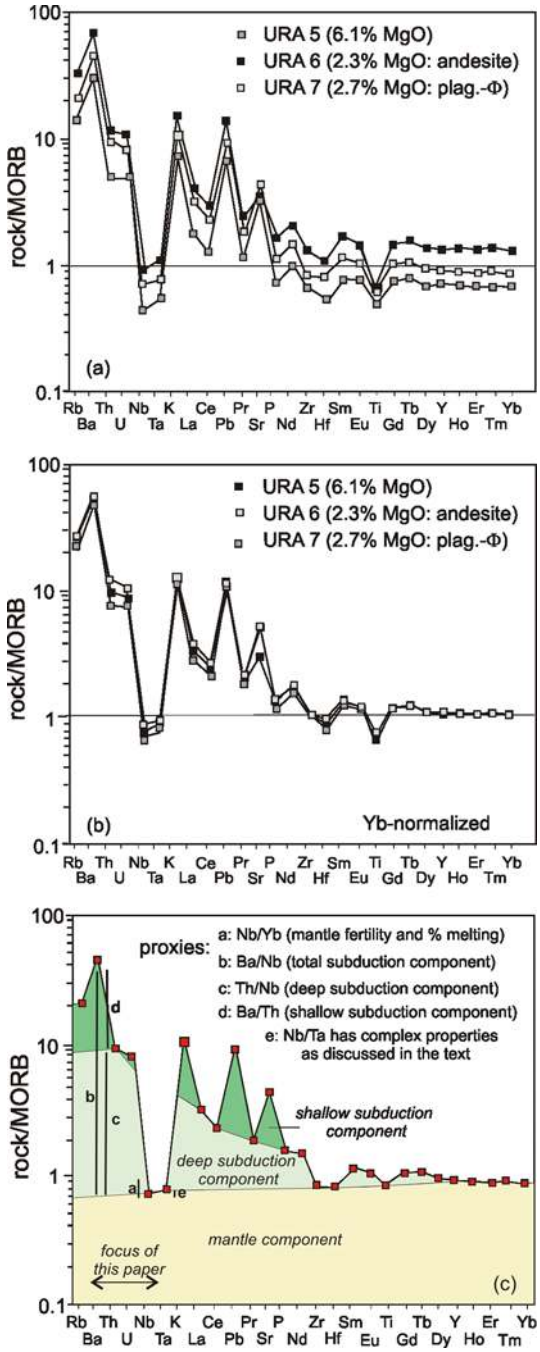

Figure 2. (a and b) Yb normalization as a means of reducing fractional crystallization and cumulation effects. The figure shows, as an example, three lavas from Uracas volcano [from *Elliott et al.*, 1997], one (URA5) relatively basic, one (URA7) highly porphyritic, and one (URA6) relatively evolved. Yb normalization brings the diverse patterns close together. (c) Geochemical pattern for a Mariana arc basalt (from Guguan) broken up into its various components (asthenosphere, deep subduction, and shallow subduction) to illustrate the choice of geochemical proxies for the different components.

(low). Where the circles overlap, the color in the overlap zone represents the mean of the overlapping data points. Scaling the maps presents a difficult choice. Linear scales would reflect the fact that addition of the subduction component is a linear process. Logarithmic scales would reflect the fact that dynamic melting and melt extraction are highly non-linear. Expanding the two ends of the range may reflect the fact that the distribution of each element ratio in the arc-basin system is bimodal, with the basin at one mode and the arc at the other. We use logarithmic scales for most element ratio maps, but a linear scale for Nb/Ta where the range of values is small. These ratio maps highlight a series of features within the Mariana arc-basin system. Here, we first use them to discuss variations in enrichment and depletion of mantle sources (Ta/Yb), then to discuss the total addition of subduction components (Ba/Ta), and finally to determine how processes responsible for adding the subduction component vary along and across strike of the system (Th/Ta, Nb/Ta, Ba/Th).

4.2.1. Mapping Mantle Enrichment and Depletion Using Ta/Yb Ratios

[18] In the Ta/Yb map (Figure 3a), to a first approximation, the highest values represent melts from the most enriched mantle and the lowest values represent melts from the most depleted mantle. The map therefore indicates that depleted mantle underlies most of the arc except the N-NSP. The most enriched mantle underlies the NSP and irregular locations within the Mariana Trough. Note that except at its extremities, the Mariana Trough is more enriched than average N-type MORB (which has a Ta/Yb ratio of about 0.04 [*Sun and McDonough*, 1989]). Ta/Yb is, of course, also sensitive to variations in degree of melting, but this only has a significant impact when garnet is residual or the degree of melting is small. In this case, there is no evidence of residual garnet in any sample, nor of very low degrees of melting [e.g., *Stolper and Newman*, 1994; *Gribble et al.*, 1998], so it is likely that these variations are primarily highlighting source variations.

4.2.2. Mapping Total Subduction Enrichment Using Ba/Ta Ratios

[19] The Ba/Ta map (Figure 3b) depicts the total subduction enrichment. It highlights the high proportion of subduction component in the arc magma source compared to the source of back-arc basin basalts. The Mariana Trough does, however, have a

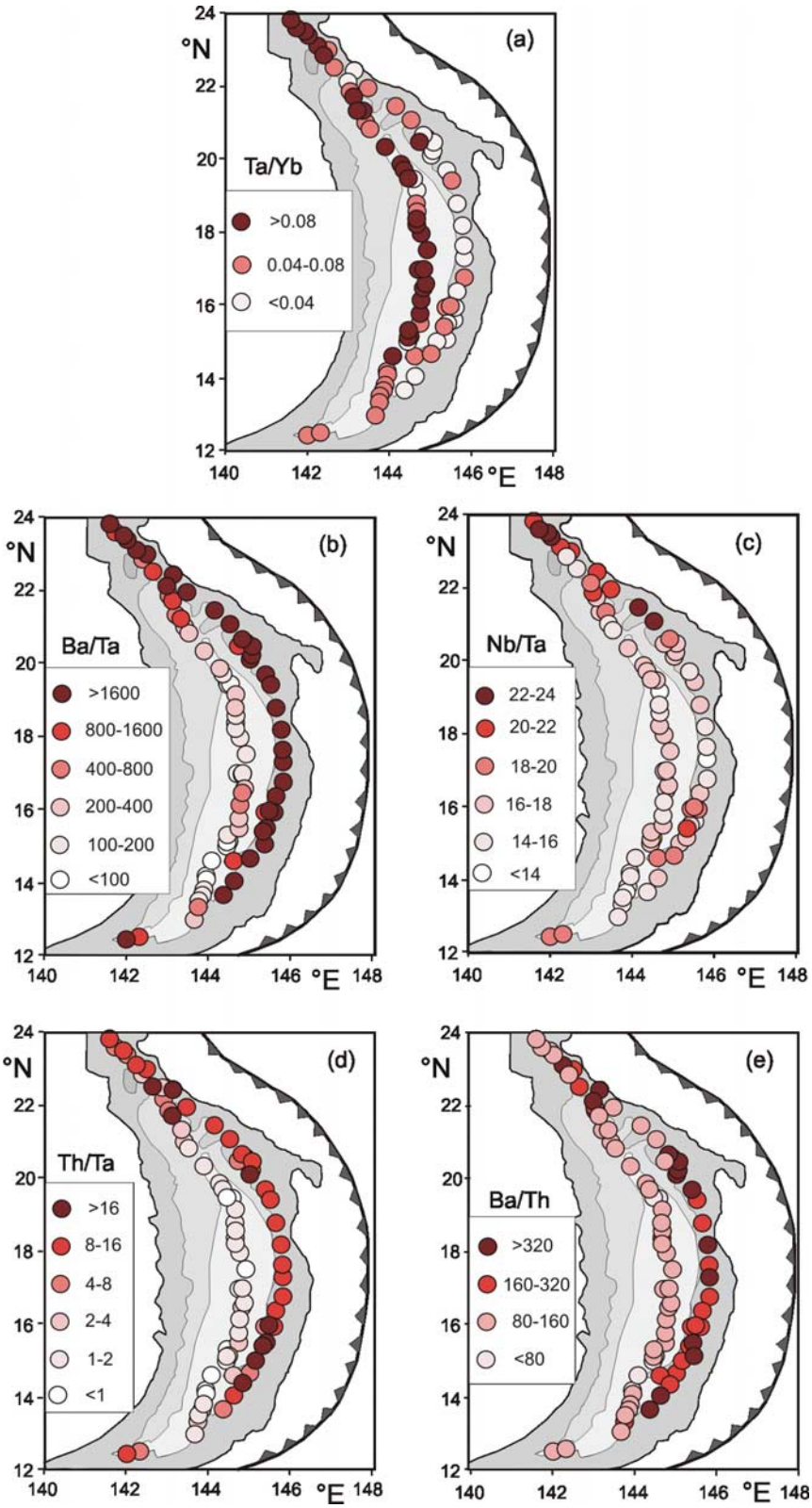

Figure 3. Geochemical ratio maps for (a) Ta/Yb, (b) Ba/Ta, (c) Nb/Ta, (d)Th/Ta, and (e) Ba/Th, highlighting mantle composition and the various types of component addition to the mantle wedge. For a subduction system in a given thermal state, Ta/Yb is a proxy mainly for mantle fertility, Ba/Ta is a proxy for total subduction addition, Nb/Ta is a proxy for ultradeep subduction, or mantle-derived, small-degree melt addition, Th/Ta is a proxy for deep subduction addition, and Ba/Th is a proxy for shallow subduction addition.

significant subduction component in the NVTZ, where it verges on the arc and "captures" the arc magmatic supply. There is a comparable increase where the Mariana Trough converges on the arc in the south and the highest values are reached at the southern edge of the basin at 142°E. Of particular significance is the observation that the Mariana Trough has just three areas with Ba/Ta < 100 and thus no to very little subduction input: one in the south at about 14–15°N, and two in the center of the basin at about 17.5°N and 19.5°N.

4.2.3. Mapping the Nb-Th-Ba Component Using Nb/Ta Ratios

[20] If Ta and Nb are immobile elements, the Nb/Ta map (Figure 3c) should duplicate many of the features of Figure 3a, although with a lower resolution because Nb and Ta only differ slightly in incompatibility whereas Nb and Yb differ significantly. This duplication is evident in the NSP and parts of the SSP where both Ta/Yb and Nb/Ta are high, and also in the CIP where both Ta/Yb and Nb/Ta are low and Nb/Ta ratios of <10 have been reported by *Elliott et al.* [1997]. However, the correlation is less obvious in the back-arc basin, where Ta/Yb is high while Nb/Ta is average. If these variations resulted from decoupling of Nb and Ta in the subduction zone, it would have required a high temperature for either element to be mobilized; i.e., it would have to have been ultradeep in the case of the Mariana system. If it took place in the mantle, it would have required very low degrees of melting. These possibilities will be examined in subsequent sections.

4.2.4. Mapping Deep Subduction Enrichment Using Th/Ta Ratios

[21] The Th/Ta map (Figure 3d), depicts only the deep subduction enrichment, Th having low-mobility at low temperatures (and hence shallow depth) in the Mariana system. Superficially it resembles the Ba/Ta map, as both highlight the high subduction component in subarc mantle and the areas of mantle in the Mariana Trough that have evaded subduction addition. However, there is not a perfect correlation between Ba addition and Th addition, a distinction which is better studied through the Ba/Th ratio in Figure 3e.

4.2.5. Mapping Shallow Subduction Enrichment Using Ba/Th Ratios

[22] The Ba/Th map (Figure 3e) depicts the shallow subduction component. The highest values are in the arc, primarily the central part (the CIP and SSP). Values in the Mariana Trough are typically low, indicating minor addition of a low-temperature subduction component. The notable exceptions are high ratios at the extremities of the basin, where the spreading axis converges on the arc and so may extend beneath the shallower parts of the subduction zone.

[23] The basic element ratio maps thus highlight a series of spatial geochemical relationships which require explanation. These include the patchy distribution of subduction-free mantle within the Mariana Trough, the apparently fertile mantle and high Nb/Ta of the NSP, and the increase in subduction component toward the northern and southern margins of the Mariana Trough. It is, however, possible to carry out more sophisticated mapping by trying to isolate, quantify and map the various components independently. In particular, we need to evaluate the null hypothesis, that Nb is immobile within the system. This is carried out in the Sections that follow.

5. Geochemical Mapping Using Subduction Inputs

5.1. Quantification of the Subduction Inputs

[24] The subduction inputs manifest themselves as distinctive fractionations of incompatible element ratios. However, it is important to ensure that these fractionations do result from subduction and not mantle wedge processes. In order to evaluate and map subduction inputs, we must therefore first identify the non-subduction variations. To do this, we define the MORB array using samples from the same mantle domain containing no subduction component. Because the global MORB array includes regional variations, the optimum approach is to identify the local MORB array. For the Mariana Trough, we selected the most MORB-like analyses from the spreading portions of the Mariana Trough together with MORB from the now-extinct (45–50 Ma) spreading axis of the West Philippine Basin (Table 4). These samples form a single, well-defined array. It is thus likely that there is a regional mantle domain which has supplied asthenosphere to the Mariana arc-basin systems since the Eocene. We use these Mariana Trough samples to define the MORB array and quantify the subduction inputs. Appendix A presents the MORB arrays and summarizes the

Table 4. Geochemical Data on DSDP Leg 31 and 59 MORB and OIB Samples From the West Philippine Basin Used to Help Construct the Regional MORB Array and Hence Quantify the Subduction Zone Addition to the Mantle Wedge[a]

Leg	31	31	31	31	31	31	59	59	59	59
Hole	291	291	292	292	292	294	447A	447A	447A	447A
Core	5R-2	5R-2	42R-2	45R-2	46R-1	7R-1	17R-3	18R-1	22R-3	25R-1
Cm	31–33	129–132	69–71	80–82	88–90	101–103	129–132	83–85	18–20	58–60
SiO_2	48.50	48.52	49.60	48.36	49.31	48.37	50.22	50.65	50.69	46.93
TiO_2	1.17	1.12	2.78	2.78	2.64	2.20	1.24	1.24	1.05	0.80
Al_2O3	14.95	14.44	13.45	13.31	14.30	15.71	14.55	14.63	13.80	15.77
Fe_2O3	11.72	11.21	13.67	14.86	12.60	7.82	11.25	10.69	10.41	9.14
MnO	0.16	0.18	0.16	0.17	0.20	0.09	0.18	0.18	0.18	0.14
MgO	5.93	6.65	5.11	3.56	5.01	4.65	7.51	7.54	9.35	10.28
CaO	12.47	12.67	8.99	10.04	9.39	10.32	12.08	11.84	11.87	11.15
Na_2O	2.24	2.30	3.24	3.22	3.71	3.06	2.31	2.40	2.23	2.31
K_2O	0.42	0.32	0.56	0.64	0.81	2.18	0.37	0.39	0.04	0.06
P_2O5	0.11	0.12	0.42	0.33	0.40	0.45	0.09	0.11	0.09	0.06
LOI	1.39	1.62	0.61	0.78	0.82	3.83	0.71	0.50	0.79	1.40
Total	99.06	99.15	98.59	98.06	99.19	98.69	100.51	100.16	100.49	98.04
Sc	42.8	41.9	33.8	28.5	26.1	21.9	44.0	43.3	37.3	34.2
V	303	296	321	321	306	259	339	332	319	213
Cr	346	342	69	74	74	114	208	199	326	455
Co	52.5	50.0	42.7	46.7	48.1	21.6	55.1	54.2	46.6	48.2
Ni	112	172	22	20	28	73	112	119	125	247
Cu	112	115	59	70	63	36	68	85	95	90
Zn	82	78	102	108	114	91	92	86	76	49
Ga	15.8	15.2	20.4	20.5	21.0	21.3	15.5	16.0	14.9	13.3
Rb	8.69	6.25	8.26	10.83	10.26	45.72	5.86	5.45	0.71	0.87
Sr	139	137	316	321	323	373	98	100	82	132
Y	26.9	27.0	35.4	35.9	39.4	32.3	33.6	34.1	28.2	21.0
Zr	73.8	70.5	193.0	186.7	212.8	193.6	68.2	69.1	52.6	54.5
Nb	6.27	5.83	24.07	23.35	26.38	51.37	1.68	1.70	1.14	1.39
Ba	36.4	30.4	148.5	140.5	163.3	446.6	8.1	7.6	5.8	7.1
La	4.95	4.62	18.46	17.81	21.21	30.52	2.43	2.47	1.75	2.18
Ce	12.30	11.50	41.94	40.62	47.86	58.95	7.77	7.81	5.76	6.75
Pr	1.76	1.66	5.42	5.19	6.18	6.86	1.33	1.35	1.04	1.10
Nd	9.10	8.72	25.38	24.21	28.43	29.49	7.89	7.85	6.28	6.05
Sm	2.77	2.64	6.16	6.03	6.83	6.17	2.81	2.91	2.35	1.98
Eu	0.98	0.93	2.04	2.03	2.20	1.94	1.01	1.03	0.86	0.77
Gd	3.63	3.50	7.00	6.91	7.79	7.10	3.93	3.99	3.37	2.72
Tb	0.67	0.64	1.08	1.08	1.17	0.97	0.77	0.79	0.66	0.50
Dy	4.38	4.25	6.35	6.43	6.88	5.60	5.22	5.30	4.44	3.35
Ho	0.96	0.92	1.26	1.27	1.37	1.10	1.15	1.17	0.98	0.72
Er	2.74	2.71	3.41	3.47	3.66	2.99	3.34	3.41	2.85	2.08
Tm	0.44	0.44	0.51	0.53	0.56	0.45	0.54	0.56	0.47	0.34
Yb	2.67	2.70	3.02	3.19	3.37	2.75	3.33	3.43	2.87	2.07
Lu	0.43	0.42	0.46	0.48	0.52	0.42	0.53	0.54	0.45	0.33
Hf	1.93	1.84	4.61	4.45	5.08	4.36	1.95	1.96	1.56	1.39
Ta	0.41	0.37	1.54	1.51	1.69	3.15	0.12	0.12	0.08	0.09
Pb	0.47	0.63	0.74	2.83	1.60	3.13	0.56	0.40	0.24	0.40
Th	0.47	0.45	2.05	1.99	2.34	4.96	0.14	0.14	0.10	0.11
U	0.16	0.14	0.56	0.56	0.70	0.98	0.89	0.52	0.03	0.04

[a] Oxides in wt.%; trace elements in parts per million; LOI, loss on ignition; total iron quoted as Fe_2O_3.

methodology used to quantify the deviations from the arrays.

[25] Figure 4 contains the plots used to quantify the proportion of subducted elements in the mantle source to the lavas of the Mariana arc-basin system. Figures 4a–4c highlight displacements from the MORB array for the elements Ba, Nb and Th. The contours give the percentages of each of these three elements in the mantle source that can be attributed to subduction, assuming that both Ta and Yb are conservative (subduction-immobile) elements. Figure 4d highlights the displacement of Ba from the MORB and deep subduction arrays.

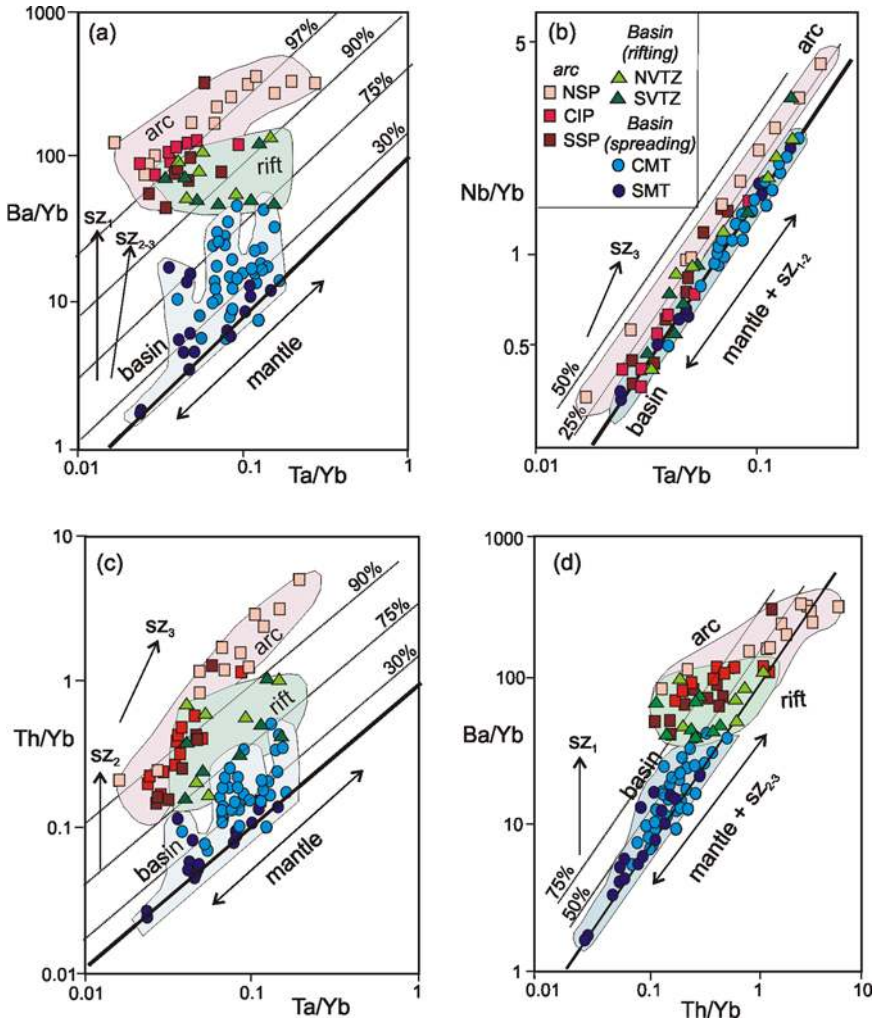

Figure 4. Plots showing deviations from the MORB arrays on element ratio diagrams given as the percentage contribution of the subduction-mobile element to the mantle source. (a) Ba displacement relative to Ta is a proxy for total subduction addition, (b) Nb displacement relative to Ta is a proxy for ultradeep subduction addition, (c) Th displacement relative to Ta is a proxy for deep subduction addition, and (d) Ba displacement relative to Th is a proxy for shallow subduction addition. The labels sz_1, sz_2, and sz_3 refer to the Ba-only, Th-Ba, and Nb-Th-Ba subduction components, respectively, as discussed in the text. Contours parallel to the MORB arrays on plots of M_1/Yb versus M_2/Yb refer to the percentage of subduction-derived element M_1 in the mantle source, assuming that M_2 is subduction-immobile ($= \Delta M_1 - M_2$). On the Ba/Yb-Th/Yb plot they refer to the percentage of shallow subduction-derived Ba, assuming (as the data indicate) that the deep subduction vector is subparallel to the MORB array.

The contours give the percentage of Ba in the mantle source that can be attributed to shallow subduction, assuming that Th is immobile in shallow (low-T) subduction fluids. If Th always has some mobility, then these percentages will be underestimates of the true shallow component.

[26] Figures 4a–4c thus highlight the selective additions of the more subduction-mobile elements to the mantle wedge. Ba, the most subduction-mobile element, provides the greatest displacement of the arc from the MORB array and is most sensitive to subduction additions to the back-arc basin (Figure 4a). The contours demonstrate that over 90% of the Ba in the mantle source of the arc lavas is subduction-derived, with the NSP having the highest values. The spreading part of the Mariana Trough (SMT and CMT) has 0–75% as subduction-derived, and the rifting part of the Mariana Trough (the NMT) has intermediate values. Th reveals a similar enrichment pattern but with somewhat smaller displacements (Figure 4c). More surprising is the fact that arc lavas from the NSP are displaced from the MORB array on the Nb-Ta diagram (Figure 4b). By contrast, the vast majority of Mariana Trough spreading lavas, and

CIP and SSP arc lavas, plot along the MORB array. Thus, unless melting leaves a residual phase which fractionates Nb from Ta [*Sun and Stern*, 2001], a Nb-bearing fluid or melt component must have contributed to the source of the northern Mariana arc lavas. The Ba-Th diagram in Figure 4d shows that the mantle array and the deep-subduction trend (best exemplified by Mariana Trough Segments 2–3) follow very similar trends with slopes close to unity. Shifts above this array are then a function of shallow addition of Ba (but not Th) to mantle modified by deep subduction components. The contours show that up to 90% of the Ba in some arc lavas owes its origin to this shallow subduction component, although other arc lavas contain no shallow component.

[27] In Figure 4, there are several trends of interest. The methodology for interpreting these trends has been described by *Pearce et al.* [1995]. Trends parallel to the MORB array can be explained by the processes which influence the MORB array, namely, source mixing, dynamic melting and melt extraction during flow. Vertical trends can be explained by variable subduction component addition to a given mantle source. Trends shallower than the MORB array can usually be explained by subduction addition to a variable mantle source. Trends steeper than the MORB array can usually be explained by mixing of mantle containing different proportions of both mantle and subduction components.

[28] From this, it is apparent that the Mariana Trough segments that form vertical arrays in Figures 4a and 4c experience variable Ba and Th addition, but little or no Nb addition, to the mantle source. This is particularly clear in the northern part of the CMT (Segments 2–3) and the SMT (Segments 17–18). In Figure 4b, the displacement from the MORB array for some arc samples requires a Nb-bearing component, although addition of this component gives a diagonal, rather than vertical, vector as Ta must be mobile as well as Nb. However, the MORB-parallel trend followed by the NSP is characteristic of mantle, rather than subduction, processes; i.e., it is attributable to mantle enrichment and depletion processes, or to dynamic melting. To preserve this trend, the Nb-bearing subduction component must be added before the mantle processes operate.

[29] Similarly, the MORB-parallel trend exhibited by the NSP in Figure 4c could be explained by Th addition followed by mantle depletion and dynamic melting. By contrast, the diagonal trend in Figure 4c followed by some SSP and CIP lavas is better explained by source mixing. The shallow trends followed by arc and rifting lavas on the Ba-based diagrams of Figures 4a and 4d could be explained by mixing, or by addition of a subduction component to variably depleted mantle, or by mantle depletion combined with addition of the Ba-rich subduction component. Overall, therefore, the causes of displacement of the compositions from the MORB array are varied and complex. At least some of the Mariana arc cannot therefore be explained simply in terms of the addition of two subduction components (fluid and melt) to a mantle source.

5.2. Mapping the Mariana Arc-Basin System Using Subduction Additions

[30] Figure 5 gives the geochemical maps based on subduction additions as quantified in Appendix A and illustrated in Figure 4. The subduction additions represent the percentage of a given element in the mantle source that is derived from the subduction zone. The symbol $\Delta M_1 - M_2$ indicates that the values are calculated for the mobile element M_1 assuming the element M_2 is immobile. Each of the maps highlights a particular feature according to the proxy used.

5.2.1. Mapping Total Subduction Input Using Ba Addition Relative to Ta

[31] This map (Figure 5a) is predictably almost identical to Figure 3b, the Ba/Ta map. It is particularly effective in highlighting the three parts of the Mariana Trough without subduction components: around 14–15°, 17.5° and 19.5°N. It also illustrates the much higher Ba enrichment in the arc (always >95% subducted Ba) compared to the basin (always <90% subducted Ba) and the increase in subduction component within the basin at the basin edges.

5.2.2. Mapping the Nb-Bearing Subduction Input Using Nb Addition Relative to Ta

[32] The Nb-Ta map (Figure 5b) benefits particularly from the "subduction addition" approach as Nb/Ta can be fractionated significantly both by melting and enrichment processes. By using deviations from the mantle array, the melting process is largely eliminated and the map can then focus on enrichment processes. The map is therefore different in detail from the Nb/Ta map in Figure 3c in that it lacks the variability within the Mariana

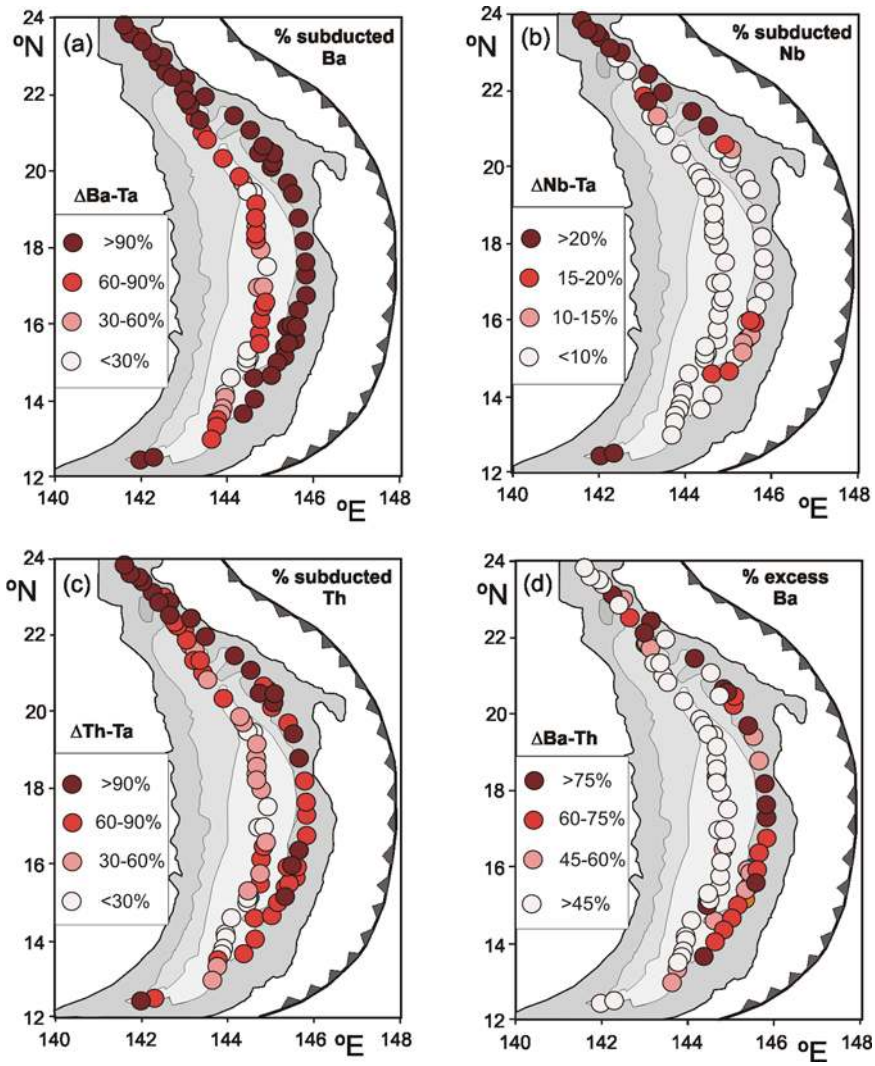

Figure 5. Geochemical maps showing the deviations from the MORB arrays illustrated in Figure 4. As in Figure 4, (a) Ba displacement relative to Ta is a proxy for total subduction addition, (b) Nb displacement relative to Ta is a proxy for ultradeep subduction addition, (c) Th displacement relative to Ta is a proxy for deep subduction addition, and (d) Ba displacement relative to Th is a proxy for shallow subduction addition. $\Delta M_1 - M_2$ is defined in the caption for Figure 4.

Trough caused by mantle enrichment and depletion. The Mariana Trough has MORB-like Nb/Ta with insignificant deviations from the MORB array except at its intersection with the arc in the north. Within the arc, the NSP has uniformly high ratios. Most of the CIP (including almost all the CIP studied by *Elliott et al.* [1997]) and much of the SSP have values within the MORB array. However, two areas of the SSP, at 12.5° and 14.5°–16°N, include elevated values.

5.2.3. Mapping Deep Subduction Input Using Th Addition Relative to Ta

[33] The ΔTh-Ta map (Figure 5c) predictably resembles the Th/Ta ratio map in Figure 3d, any differences reflecting the different scaling. It thus highlights the fact that the NSP has the greatest contribution of subducted Th to the mantle source, and emphasizes the three areas of the Mariana Trough with ΔTh-Ta <30% which lack significant subduction input.

5.2.4. Mapping the Shallow Subduction Input Using Ba Addition Relative to Th

[34] The ΔBa-Ta map (Figure 5d) resembles the Ba/Ta map in Figure 3d and so also demonstrates that excess Ba (shallow subduction addition) is greatest in the central and southern part of the arc. The Mariana Trough only has significant excess Ba in its northern and southern intersections

with the arc, with the exception of a few isolated high Ba values.

[35] The subduction-addition plots have some advantages over element ratios. Although the differences in bulk partition coefficients between Ba, Th, Nb and Ta are small, they are not always insignificant and this type of plot largely eliminates the effects of these differences. In particular, the Nb-Ta subduction-addition plot is more effective in highlighting Nb additions than the ratio plots. For Ba-Ta, Th-Ta and Ba-Th, the magnitude of the subduction additions is sufficiently high relative to mantle fractionations that the ratio plots are relatively reliable, though they do have some loss of resolution compared to the subduction-addition approach.

6. Geochemical Mapping of Source Components

6.1. Identification of Components

[36] The plots in Figure 5 reveal that at least three apparent subduction zone components augment the mantle in contributing to magma genesis in the Mariana arc-basin system: a Nb-Th-Ba component (sz_3 in Figure 4) which forms a diagonal trend on the Th-Ta plot and a displacement from the MORB array on the Nb-Ta plot; a Th-Ba component (sz_2 in Figure 4) which forms a vertical trend on the Th-Ta plot and no displacement from the MORB array on the Nb-Ta plot; and a Ba-only component (sz_1 in Figure 4) which gives a vertical displacement from the array formed by other components on a Ba-Th plot.

[37] Figure 6a (Th/Ta against Nb/Ta) combines the evidence from the Th-Ta and Nb-Ta plots and demonstrates on a single diagram the distinction between the Nb-Th-Ba component (seen in the arc and rift samples which approximately follow the diagonal sz_3 vector) and the Th-Ba component (seen in spreading basin samples which approximately follow the vertical sz_1 vector). Figure 6b illustrates how the geochemical pattern for a typical NSP sample may be broken down into four components: an asthenosphere component, a deep-subduction (Th-Ba-bearing) component, a shallow-subduction (Ba-bearing) component and the Nb-Th-Ba-bearing component. We have tentatively interpreted the latter as a lithospheric component for reasons explained in the next section.

[38] If the Nb-Th-Ba component is a lithospheric component, then it has to be subtracted numerically

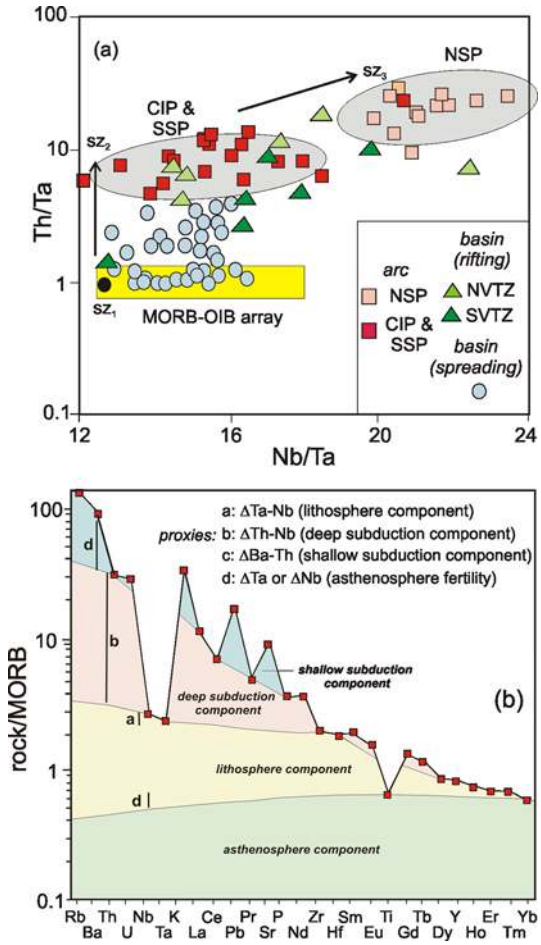

Figure 6. Graphical evidence for the four-component model for the Mariana arc-basin system. (a) Evidence for the presence of a Nb-Th-Ba component with high Nb/Ta affecting the Northern Seamount Province and lavas from the Volcano-Tectonic Zone of the Mariana Trough. (b) Typical geochemical pattern of a Nb-rich lava, illustrating how it can be broken down into four components (asthenosphere, lithosphere, deep subduction input, and shallow subduction input).

in order to interpret the Mariana system in terms of present-day subduction processes. We have described one method of doing this in Appendix B. Figure 7 applies this method to equivalent plots to those in Figure 4, but with the Nb-Th-Ba component removed and Table 5 gives data for the northern part of the Mariana arc before and after component subtraction. The effects of lithosphere component removal are striking. The arc now has Ta/Yb ratios which are comparable to, or lower than, the ratios in the spreading parts of the basin. The part of the Mariana Trough spreading center that has "captured" the arc now plots predominantly within the arc field. The spreading part of the Mariana Trough now extends to the arc field;

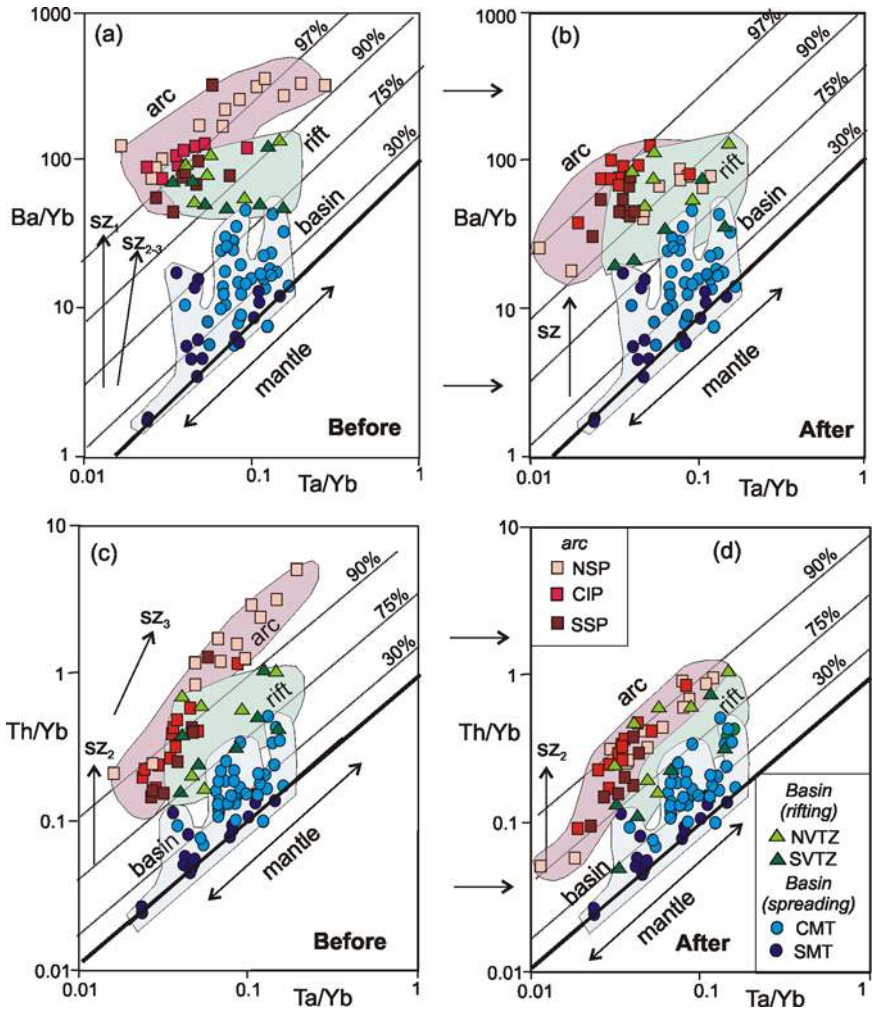

Figure 7. Plots comparing deviations from the MORB arrays on Ba-Ta and Th-Ta diagrams before and after the Nb-Th-Ba component has been mathematically subtracted as described in Appendix B and documented for some arc lavas in Table 5. Comparison of the two sets of plots illustrates the importance of the Nb-Th-Ba component in the composition of many Mariana arc and arc-rifting lavas. After component subtraction, the NSP have similar to lower concentrations of the subduction-mobile elements, Ba and Th, compared to the CIP and SSP.

i.e., the arc-basin bimodality has disappeared. On the Ba-Ta diagram, the NSP changes from having the highest, to having the lowest, Ba/Yb ratios, which is more in keeping with its greater depth to the subduction zone (Figure 1). Using the original and Nb-Th-Ba component-subtracted data, we can now investigate and map the mantle and the three enrichment components in more detail.

6.2. Mapping of Components

6.2.1. Mapping the Asthenosphere Component

[39] Although we mapped the mantle composition in Figure 3a using Ta/Yb as a proxy for mantle fertility, the fact that Nb is enriched in many arc and rift lavas from the Mariana arc-basin system means that Ta must also be enriched, i.e., that mantle fertilities may have been enhanced relative to their asthenospheric values. Thus the true picture of asthenosphere composition means that Figure 3a must also be redrawn after subtracting the Ta added in the Nb-Th-Ba component using the methodology in Appendix B. Thus we have recalculated Ta/Yb ratios for samples with Nb/Ta ratios above the mantle array. Note, however, that we only recalculated lavas with >5% added Nb so that the correction did not introduce unnecessary error.

[40] Figure 8a gives the map of corrected ratios. The N-MORB Ta/Yb ratio is 0.04, so that pale

Table 5. Effects of Subtraction of the Nb-Th-Ba Component From Compositions of Lavas From the Northern Mariana Arc Using the Methodology in Appendix B[a]

		Measured Data Before Subtraction of Nb-Th-Ba Component							Data After Subtraction of Nb-Th-Ba Component				
Volcano	Sample	Province	Ba	Th	Nb	$Ta)_{PP}$	Ta	Nb/Ta	Ba	Th	Nb	Ta	Nb/Ta
CHER	10-1-2	CIP	271	1.32	1.58	0.116	0.102	15.49	214	1.07	1.39	0.096	14.44
AHYI	15-3-2	CIP	243	0.69	1.15	0.067	0.076	15.12	200	0.58	1.03	0.072	14.23
AHYI	15-3-3	CIP	226	0.47	1.06	0.061	0.069	15.36	171	0.37	0.91	0.064	14.14
AHYI	16-3	CIP	103	0.61	0.68	0.039	0.043	15.81	70	0.43	0.55	0.039	14.14
MAKH	18-9	CIP	267	2.73	3.40	0.162	0.206	16.50	186	1.97	2.81	0.188	14.95
NWUR	19-3-5	CIP	162	0.37	0.78	0.043	0.045	17.33	72	0.18	0.50	0.036	13.85
DAIK	29-2-2	SNSP	556	4.07	4.70	0.243	0.221	21.27	130	1.09	2.19	0.152	14.46
EIFU	30.6	SNSP	389	3.12	2.83	0.142	0.127	22.28	77	0.72	1.21	0.083	14.51
EIFU	30.7	SNSP	430	3.34	2.87	0.134	0.134	21.42	101	0.89	1.34	0.092	14.57
EIFU	30.8	SNSP	470	4.45	3.25	0.166	0.152	21.38	111	1.20	1.53	0.105	14.59
EIFU	31.1.4	SNSP	310	2.80	2.38	0.126	0.111	21.44	71	0.73	1.10	0.076	14.48
EIFU	31.1.6	SNSP	304	2.31	1.98	0.103	0.092	21.52	66	0.57	0.89	0.062	14.33
EIFU	31.2.2	SNSP	456	3.58	3.29	0.162	0.150	21.93	96	0.87	1.45	0.100	14.51
FUKJ	34-2-2	SNSP	353	2.51	2.05	0.079	0.101	20.30	95	0.76	1.02	0.072	14.27
FUKY	38-2	SNSP	173	0.31	0.49	0.021	0.024	20.42	37	0.08	0.22	0.016	13.45
ICHI	44-1-5	SNSP	430	2.26	2.66	0.147	0.134	19.85	127	0.74	1.40	0.098	14.31
NIKK	45a	SNSP	171	0.52	1.17	0.056	0.056	20.89	36	0.13	0.52	0.037	13.79
KHIY	47-1-1	NNSP	790	7.43	6.81	0.267	0.283	24.06	124	1.38	2.59	0.175	14.79
SHIY	49-1-2	NNSP	684	8.79	8.06	0.421	0.369	21.84	168	2.45	3.87	0.256	15.09
CHIY	51-3	NNSP	648	3.90	4.57	0.208	0.191	23.93	100	0.71	1.71	0.117	14.60
CHIY	52-1-1	NNSP	838	7.73	7.10	0.315	0.328	21.65	216	2.26	3.50	0.231	15.17
CHIY	52-3-1	NNSP	751	7.43	8.28	0.403	0.383	21.62	205	2.28	4.20	0.273	15.38
NHIY	53-1-3	NNSP	827	18.10	13.80	0.630	0.663	20.81	278	6.72	7.82	0.499	15.66
FUKT	55-1-2	NNSP	600	3.83	6.15	0.297	0.267	23.03	120	0.89	2.66	0.176	15.10
FUKT	57-6	NNSP	579	4.71	3.31	0.143	0.149	22.21	120	1.13	1.45	0.099	14.65

[a] CHER, Cheref; AHYI, Ahyi; MAKH, Makhahnas; NWUR, NW Uracas; DAIK, Daikoku; EIFU, Eifuku; FUKJ, Fukujin; FUKY, Fukuyama; ACHI, Ichiyo; NIKK, Nikko; KHIY, Ko-Hiyoshi; SHIY, South Hiyoshi; CHIY, Central Hiyoshi; NHIY, North Hiyoshi; FUKT, Fukutoku. CIP, Central Island province; SNSP, Southern Northern Seamount Province; NNSP, Northern Northern Seamount Province. Data are from *Peate and Pearce* [1998], except that Ta has been remeasured by ICP-MS using long count times; the original Ta data (Ta_{PP}) are included for comparison with the new data. The "before and after" comparison emphasizes the importance of the Nb-Th-Ba component in the northern part of the arc (and Mariana Trough). Note that the calculations involve assumptions in estimating the component addition vectors and therefore are only approximations.

pink symbols indicate an asthenospheric source that is depleted relative to a N-MORB source, whereas the darker symbols indicate a more enriched source. Thus it is apparent that the arc is depleted except for the northern and southern extremities. In contrast, the Mariana Trough shows the reverse pattern, being enriched except at its extremities.

6.2.2. Mapping the Nb-Th-Ba (Lithosphere) Component

[41] Figure 5a (the map of ΔNb-Ta) remains a good expression of the distribution of the Nb-Th-Ba component. However, it will have underestimated the extent of Nb addition because of the assumption that Ta was immobile. If we again take a Nb/Ta gradient of 2 to reflect variable addition of this component, then the extent of Nb addition must be revised upward using the methodology in Appendix B. Figure 8b gives the corrected map for Nb addition and hence the lithosphere component. The distribution of lithosphere component is the same as in Figure 5a (i.e., focused in the NSP and parts of the SSP) but the proportions of added Nb in the mantle are now much higher. The results indicate that up to 60% of the Nb in the NSP may be attributed to the Nb-Th-Ba component (see also Table 5).

6.2.3. Mapping the Th-Ba (Deep-Subduction) Component

[42] We mapped the deep subduction component using Th/Ta ratios in Figure 3d and ΔNb-Ta in Figure 5c. However, we now know that there are potentially two sources of the added Th: the Nb-Th-Ba component as present in many of the arc lavas; and the effectively Nb-free (Th-Ba) component which is also present in the arc lavas and

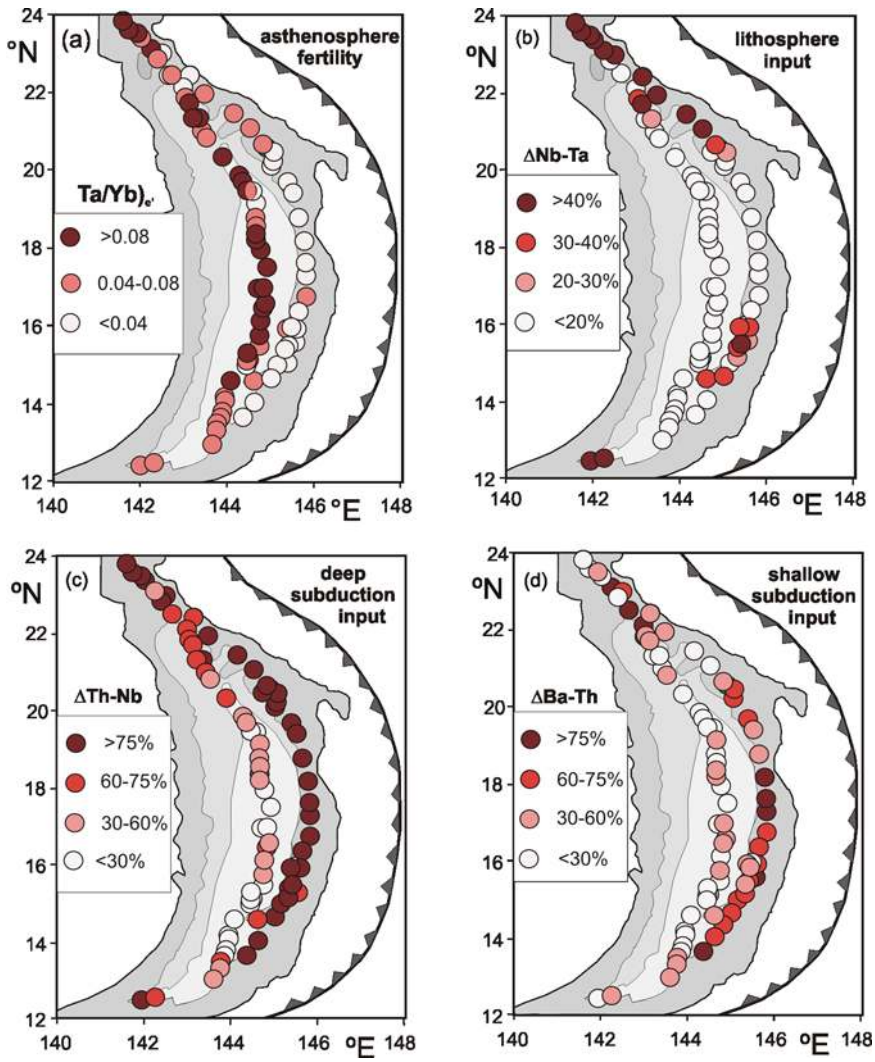

Figure 8. Component-based geochemical maps of the Mariana arc-basin system. (a) Composition of the mantle asthenosphere in terms of Ta (Ta/Yb ratio) after removal of the lithospheric component. (b) Distribution of the Nb-Th-Ba (possible lithospheric) component mapped as the % contribution of the component to the Nb in the mantle source. (c) Distribution of the Th-Ba (deep subduction) components mapped as the % contribution of Th to the mantle source after subtracting the lithospheric component. (d) Distribution of the Ba-only (shallow-subduction) component mapped as the % contribution of Ba to the mantle source after subtracting the effects of the lithospheric and deep subduction components.

many of the Mariana Trough basalts. To map the real Th-Ba component, the effects of the Nb-Th-Ba component must therefore also be subtracted as described in Appendix B.

[43] Figure 8c gives the corrected map. Now, in contrast to the earlier geochemical maps, the NSP exhibits Th enrichments which are similar in level to those of the other arc segments. The basin again exhibits the three MORB-like areas with little subducted Th addition. Interestingly, the intersection between the Mariana Trough and Mariana arc has elevated values lying between the values of the arc and basin. This supports models of a mixed arc-basin mantle source in that area.

6.2.4. Mapping the Ba-Only (Shallow-Subduction) Component

[44] We mapped the shallow (Ba-only) subduction component using Ba/Ta in Figure 3e and ΔBa-Th in Figure 5d. As with Th, we used the procedure in Appendix B to make the correction for the Nb-Th-Ba component. Figure 8d then maps the Ba-only contributions from the subduction zone to the mantle source using, as before, the Ba/Th proxy.

The new map resembles the ΔBa-Th map in Figure 5d, but the proportion of subduction-derived Ba is reduced as shown by the different scales. As before, it highlights the Ba addition to the arc and the variable, but generally small, addition to the basin source. The key observation is then that the greatest addition of the cool, shallow component (monitored by Ba) is in the center (CIP) and south (SSP) of the arc. The basin also shows interesting contrasts. Shallow subduction addition is most evident in the extreme north and south where the basin converges on the arc and the subduction zone therefore lies at shallow depth beneath the BABB source region.

7. Origin of the Mantle and Subduction Components

7.1. Origin of the Mantle Component

[45] The data highlight three locations of regional MORB mantle all in the Mariana Trough and mainly in Segments 16–13 though also in Segments 3 and 8 (Figure 9). These locations have been identified previously. In particular, *Gribble et al.* [1996] recognized the presence of N-MORB in the SMT and stressed that at least some lavas in the Mariana Trough have no subduction component and so can be explained solely by adiabatic decompression. They also noted that MORB-like Mariana Trough samples have isotopic characteristics similar to those of Indian MORB. *Hawkins et al.* [1990] found that about half of their samples in their study area from 17.7° and 18.5°N to be N-MORB and the other half to be back-arc basin basalts (BABB). The latter samples lay primarily in the south of their study area, so explaining why *Sinton and Fryer* [1987] recovered only BABB from 18°N.

[46] Our data and synthesis also indicate that the Mariana Trough MORB resemble Indian MORB mantle in their slightly elevated concentrations of LILE compared with Pacific MORB mantle and plot on the same trace element array as other MORB lavas from the Philippine Sea Plate (Figure A1, Appendix A). Note that this emphasizes the importance of choosing the correct MORB array for any calculations of subduction input. Mariana Trough MORB-like basalts are also enriched in incompatible elements relative to N-MORB. There is no evidence for the cause of that enrichment, although *MacPherson and Hall* [2001] have proposed that plume-related mantle was present in the early stages of the evolution of the Mariana system.

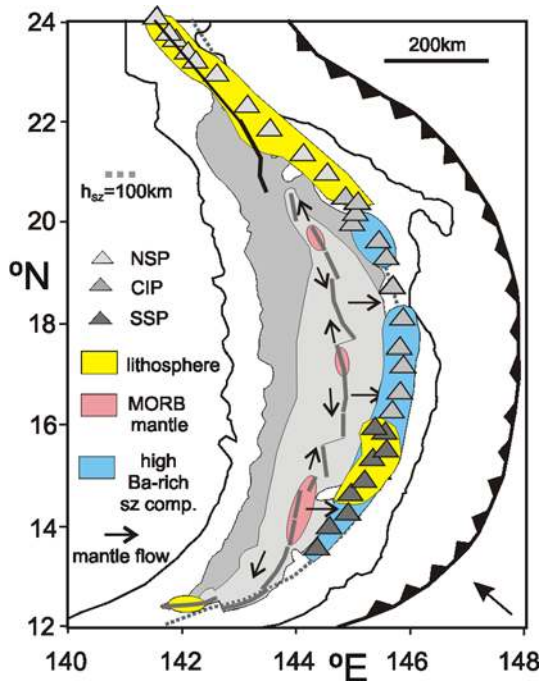

Figure 9. Summary of the key features of the geochemical maps in Figures 3, 5, and 8.

[47] By contrast, lavas from the magmatic front of the arc are almost all depleted relative to the average N-MORB of *Sun and McDonough* [1989]. This may indicate that the incoming MORB mantle subsequently experienced melt loss during flow toward the arc front as proposed by *McCulloch and Gamble* [1991] and *Woodhead et al.* [1993]. The Mariana Trough between and beyond the MORB segments is mostly enriched relative to N-MORB, though less so than the incoming MORB mantle as depicted in Figure 9. This could mean that the mantle flowed along-axis losing a melt fraction. Alternatively, there may be mixing between depleted subarc mantle and the incoming mantle as proposed by *Martinez and Taylor* [2002] and *Taylor and Martinez* [2003]. More detailed investigation of geochemical variations within ridge segments, not an objective of this paper, may help to resolve these options.

7.2. Origin of the Nb-Th-Ba Subduction Component

[48] The results of our study indicate a number of constraints on the origin of this component.

[49] 1. Nb/Ta is sufficiently high to require a subduction melt or small-degree mantle melt.

[50] 2. Th/Nb and Ba/Nb are sufficiently high to suggest a subduction contribution.

[51] 3. The geochemical maps show that this component is present in the NSP and the northernmost part of the CIP, parts of the SSP, and the NMT (Figure 9).

[52] 4. The component is most important in the NSP, where it may be the main cause of subduction enrichment. Elsewhere, it lies on what appear to be mixing lines between NSP and CIP mantle sources.

[53] 5. The CMT and SMT do not contain this component even though they may carry a high Th-Ba subduction component.

[54] Observation 2 indicates a subduction link, but observations 3–5 indicate that there is not a systematic relationship between addition of the high-Nb component and the present-day subduction geometry: otherwise the component should predominate where the subduction zone is deepest or be restricted to the northern zone of oblique subduction. Similarly, it is unlikely to be explained by the nature of presently subducting sediment, because the isotopes record a change from volcaniclastic-dominated to mixed pelagic-volcaniclastic sediment input between N-NSP and S-NSP [*Peate and Pearce*, 1998], not between the NSP and CIP where the Nb/Ta ratio changes (Table 5). Thus we believe (as already depicted in Figures 6 and 8) that this component is not linked to present-day subduction, but has an origin in the subarc lithosphere. This explains the dominance of the component in areas where the arc has just started rifting in the north and south of the arc-basin system. In that respect, arc rifting resembles continental break-up where the first magmatic products have a lithospheric origin and significant extension is needed before "normal" asthenospheric sources prevail. Other areas of enrichment, namely, the northernmost part of the CIP and the center of the SSP, are not explained by this model. They could, however, result from relict lithosphere or from mantle wedge that is contaminated by a lithospheric component.

[55] If the mantle lithosphere does act as a store for a high-Nb component, the question then arises as to the nature of the this component and how, when and why it was added to the lithosphere. The options, given the constraints listed above, are as follows:

[56] 1. It is a hot subduction component, perhaps slab or sediment melt, added under unusual conditions associated with the presubduction environment (e.g., collisions in the trench, shallowing of subduction, or oblique subduction). In this case the high Nb and high Nb/Ta may be explained by melting of subducted material in the presence of residual rutile [e.g., *Green*, 1995].

[57] 2. It represents small mantle-derived melt fractions added to the lithosphere. If these melt fractions result from addition of a Th, Ba-rich fluid to the mantle wedge, then they could derive their high Th/Nb character from the slab, but high Nb/Ta from the mantle. The involvement of carbonatite melts, which are known to have high Nb/Ta ratios [*Green*, 1995; *Hoernle et al.*, 2002], may be important. Normally these Ba, Th-rich, high Nb/Ta melts would contribute to the melting column but, if the melting column is short and arc volcanism is not taking place at the time, then the components could simply infiltrate and enrich the lithosphere.

[58] There are a number of reasons why 2) may provide the best solution. As already noted, the high Th/Ta and Ba/Ta of the lavas containing the Nb-Th-Ba component indicate that much of the Th and Ba have a subduction origin. Th-rich components elsewhere do not exhibit much Nb/Ta fractionation, however [*Münker et al.*, 2004]. Thus mantle source processes must also be important. Most obviously, the shoshonitic lavas of the NSP contain high Na, as well as K, which would support a mantle contribution. In addition, *Ito and Stern* [1985] use combined oxygen and strontium isotope systematics to infer a "most probable origin by melting of subduction-modified oceanic island or hot spot type mantle." Even for enriched mantle, however, *Eggins et al.* [1997] conclude that "any fractionation of Nb/Ta from the mantle source ratio is most likely only at tiny degrees of melting." This is supported by the fact that even the alkali basalts from the West Philippine Basin form the upper part of the MORB array with no large displacement to high Nb/Yb ratios (Appendix A). A lithospheric reservoir enriched by a succession of small melt fractions would be a much more effective way of increasing the Nb/Ta ratio of the source. We are currently investigating this hypothesis using Hf isotopes (J. D. Woodhead et al., manuscript in preparation, 2005). At present, we therefore simply note that Nb/Ta mapping may permit, for the first time in this area, the identification of areas of enriched lithosphere in the Mariana arc-basin system.

7.3. Origin of the Th-Ba Subduction Component

[59] The deep component is characterized by both Th (and LREE) and the most fluid-mobile elements

such as Ba, Rb and Sr. As Figure 8c demonstrates, this is the main component in the back-arc basin and is important throughout the arc. The component is most likely extracted from the subducted slab as a sediment-derived melt [*Elliott et al.*, 1997] or siliceous fluid [*Woodhead*, 1989].

[60] The enrichment of the deep subduction component in arc melts compared with back-arc melts probably relates simply to the proximity of the mantle to the subduction zone. The Th-Nb plot indicates that the mantle begins with a composition similar to the Mariana Trough MORB. In the north (in particular, segments 2–3), the deep subduction component is added to that composition. In the south (segments 17–18) the mantle becomes depleted, presumably during flow along the basin toward the trench, before the deep subduction component is added.

7.4. Origin of the Ba-Only Subduction Component

[61] The shallow subduction component as defined here is marked by Ba addition but no significant Th addition. The fact that it reaches its highest contribution in the center of the arc (Figure 9), with high values also in the south of the arc and where the basin and arc intersect, may indicate that the critical factor controlling the appearance of this component is the ability of the mantle to flow toward the trench so that it overlies the shallow parts of the subduction zone. In the NSP, it is possible that the incipient or early rifting of the arc allows more vertical than lateral flow of the mantle and provides little opportunity for shallow components to be added beneath the arc front; alternatively, oblique subduction may cause any Ba-rich fluid to be released before the mantle wedge asthenosphere is reached. By contrast the CIP and SSP have evolved to the stage where there is steeper subduction and the lithosphere component is still a part of the mantle asthenosphere, as explained below.

8. Implications for the Geochemical Evolution of the Mariana Arc-Basin System

[62] The distinctive feature of the Mariana convergent margin system is the presence of all stages of arc rifting through to true back-arc extension. The effects of this are evident from the geochemical mapping. The key, new observation to emerge from this study is the fact that the north and extreme south of the system, where arc rifting is in progress, have distinctively high Nb/Ta ratios. The arc in the center and south of the system, where a steady state arc-basin system has evolved, has the highest Ba/Th ratios. There is currently no unique interpretation of the unusual Nb/Ta ratios. One model consistent with the geochemical maps is illustrated in Figure 10 and outlined below.

[63] If our interpretation is correct, that the high Nb component was stored in the lithosphere, then this enrichment must predate rifting. Given that the West Mariana Ridge (the present remnant arc) has a normal calc-alkaline composition, then it is likely that this enrichment process took place during the period of reduced magmatic activity between the end of the West Mariana arc phase and the end of the rifting phase (between about 8 and 4 Ma [*Clift and Lee*, 1998]). If true, this could have coincided with a period of shallow (flat) subduction, as in the present Central Andes [e.g., *Kay and Abbrazzi*, 1996]. Alternatively, oblique subduction, which presently characterizes the NNP, may have inhibited magmatic activity. In both cases, the small-degree melts that would contribute to the melting column during a normal subduction episode could instead enrich the lithosphere (Stage 1 in Figure 10). In this illustration, small-degree asthenospheric melting is triggered by a subduction component. This is not, however, the only model to fit the trace element data. Direct derivation of a component rich in Nb, Th and Ba from the deep parts of the subducted slab cannot be ruled out, as in the *Clift and Lee* [1998] model of increased sediment subduction during rifting and slab rollback. It is also possible that lithospheric enrichment is a normal part of steady state subduction processes and so does not depend on unusual slab geometries.

[64] Once rifting begins, asthenosphere will again be able to flow into the wedge corner, ablating the preexisting lithosphere. The combination of transfer of heat and decompression can then lead to low degrees of melting of the enriched (low melting point) parts of the lithosphere during the early stages of rifting (Stage 2 in Figure 10). The shoshonites of the NSP currently represent this stage of evolution.

[65] Further rifting will then lead to further influx of asthenosphere and ablation of the lithosphere. The asthenosphere melts in response to addition of a subduction component as in normal arc volcanism, but relics of preexisting lithosphere give a mixture of mantle sources (Stage 3 in Figure 10).

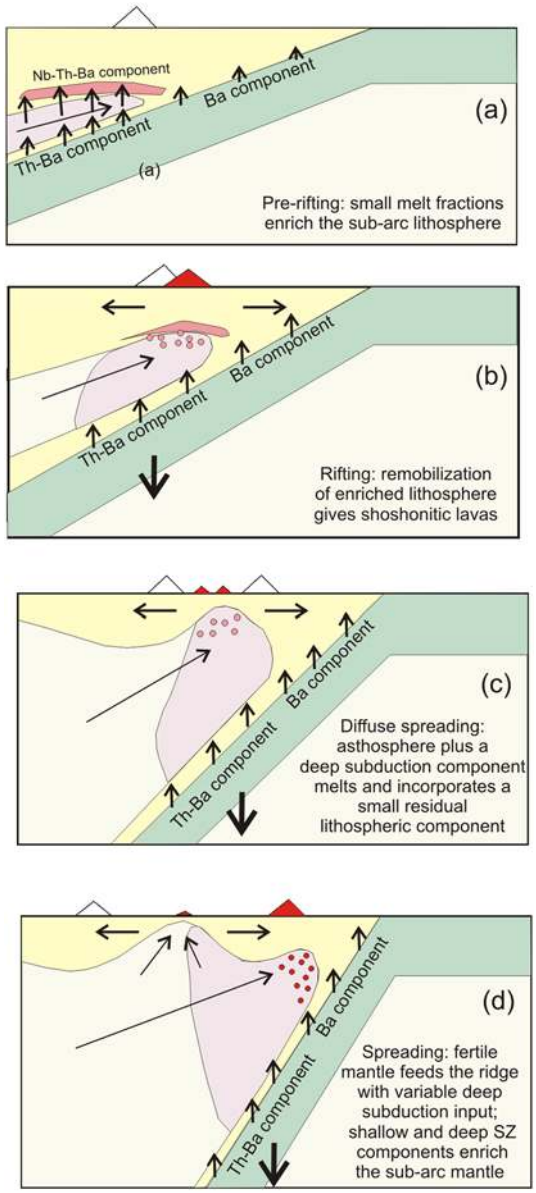

Figure 10. One possible explanation of the geochemical evolution of the Mariana system based on the component mapping presented in this paper. The diagram shows a Nb-Th-Ba component added to the lithosphere during a period of shallow slab dip and volcanic quiescence and then progressively removed during rifting and renewed arc activity. In any diagram, the shaded (red) volcanoes are active, while the unshaded (white) volcanoes are inactive. The Nb-rich component is shown in dark pink, the Th-Ba component is shown in pale pink, and the Ba-component is shown in red. Note that the unzipping of the Mariana arc means that different parts of the Mariana system have reached different stages of evolution, from rifting in the extreme north (and south) to spreading in the center.

This may be the situation in the northern CIP and parts of the SSP.

[66] Eventually, the lithosphere component is fully extracted and subduction becomes steady state, with the mantle obtaining first a deep and then a shallow subduction component as it rises to the arc front (Stage 4 in Figure 10). By incorporating a high shallow subduction component, the mantle will have high Ba/Th. This may be the situation presently observed for the central CIP, most of the SSP and the edges of the Mariana Trough. In the central part of the Mariana Trough, it is interesting to note that extension has been sufficient in three discrete sites to allow mantle unmodified by subduction to feed the back-arc basin and generate true MORB. The tectonic reason for the distribution of subduction-unmodified mantle is unclear and requires further investigation. It may be a function of back-arc ridge tectonics and the extent to which eastward ridge jumps have enabled the spreading axis to relocate toward subduction-modified mantle sources. Alternatively, it may be a function of regional tectonic factors that may favor input of "fresh" mantle, such as the unusual degree of along-strike extension of the central part of the basin, or the possible tear in the subducting plate in the south.

9. Conclusions

[67] The present database indicates that there are only three areas of MORB-like compositions in the Mariana Trough. The mantle feeding the Mariana Trough is enriched in incompatible elements relative to Depleted MORB Mantle. It is possible that mantle upwelling in these three areas then spreads north and south, becoming depleted because of melt extraction during flow or mixing with more depleted mantle.

[68] A high Nb-Th-Ba component characterized by high Nb/Ta is a ubiquitous feature of the Mariana arc in the north (NSP). Other parts of the arc (northern CIP and parts of the SSP) exhibit variable mixing between mantle containing the high Nb/Ta component and normal arc mantle. The VTZ at the northern end of the Mariana Trough similarly carries this component. We explain these variations in terms of enrichment of mantle lithosphere prior to rifting of the arc, although alternative explanations are possible. The enriched component may be a high-temperature subduction-derived melt, and/or a small-degree melt of mantle modified by a subduction component.

[69] A "deep" subduction component (the "sediment melt" component of *Elliott et al.* [1997]) characterized by Th and Ba (but no Nb) has influenced much of the Mariana Trough and all of the Mariana Arc. Probably, this is the first component added to the mantle asthenosphere as it flows toward the arc front.

[70] A "shallow" subduction component (the "fluid" component of *Elliott et al.* [1997]) is characterized by addition of Ba (but not Th or Nb) and has influenced parts of the Mariana Trough (particularly its margins) to a small extent, but is most evident in the southern and central parts of the arc. We believe that in these parts of the arc, the mantle can flow closer to the trench and so incorporate a shallower (and hence Ba-rich, Nb,Th-poor) component. The fact that this Ba addition accompanies a decrease in Th (and slight decrease in Ba) indicates that the addition of Ba accompanies melt extraction during flow within the subarc melting column.

[71] We note that the identification in this paper of the third (Nb-rich) subduction component in the Mariana arc-basin system will need to be reconciled with isotopic data. It is apparent that Sr, Nd and Pb isotopic ratios are remarkably homogeneous for the Nb-rich arc lavas [*Stern et al.*, 2003], and that oxygen isotope ratios, in particular, permit only a very small amount (c. 1%) of subducted oxygen to be involved [*Eiler et al.*, 2000; *Ito et al.*, 2003]. Hf isotopes are critical (as Hf is a high field-strength element which is also enriched in the Nb-rich lavas), though the extent of Hf mobility is subduction systems is currently controversial [*Pearce et al.*, 1999; *Woodhead et al.*, 2001]. The existence and origin of a Nb-rich component therefore requires further testing but, if present, has significant implications for magma genesis during arc evolution and arc rifting.

Appendix A: Quantifying Subduction Additions

[72] For this paper, subduction additions for any subduction mobile element are calculated as the proportion (or percentage) of that element in the mantle source that is derived from the subduction zone. They are based on deviations from a MORB array, mainly on projections of a subduction mobile element against a subduction immobile element. For most plots, Yb is used as a normalizing factor and Ta as the immobile element for reasons given in the text. For studying shallow subduction, Yb is used as a normalizing factor and Th as the immobile element. Figure A1 shows the MORB arrays for the key projections used in this paper. These have the following equations:

$$\log(\mathrm{Ba/Yb}) = 1.09\log(\mathrm{Ta/Yb}) + 1.98, \quad \text{(A1)}$$

$$\log(\mathrm{Th/Yb}) = 1.07\log(\mathrm{Ta/Yb}) + 0.12, \quad \text{(A2)}$$

$$\log(\mathrm{Nb/Yb}) = 1.05\log(\mathrm{Ta/Yb}) + 1.23, \quad \text{(A3)}$$

$$\log(\mathrm{Ba/Yb}) = 1.07\log(\mathrm{Th/Yb}) + 1.97. \quad \text{(A4)}$$

[73] A slope greater than unity in equations (A1)–(A3) indicates that all the elements listed are more incompatible than Ta. The slopes give a measure of the relative incompatibility. Including U (not shown here), the compatibility order with slopes in parentheses is Ba (1.09 = most incompatible), Th (1.07), Nb (1.05), U (1.02), Ta (1.0 = least incompatible).

[74] Deviations from these arrays then give a measure of the contribution of the subduction component to the mantle wedge source, assuming that the chosen immobile element is indeed immobile. It is possible to define the expected value of a subduction-mobile element (M_e) as the value it would have prior to subduction addition assuming it would then have lain on the MORB array. This value can then be calculated from the concentration of the subduction-immobile element (here, Ta) using the above equations. For example, for Ba:

$$\left(\frac{Ba}{Yb}\right)_e = 10^{(1.09\log(Ta/Yb)+1.98)}. \quad \text{(A5)}$$

[75] If Ba_o is the observed concentration of Ba, i.e., the Ba concentration of the wedge, and Ba_e is the Ba concentration of the mantle before subduction addition, then ($Ba_o - Ba_e$) is the Ba concentration of the subduction component. Thus the mass fraction (X) of subducted Ba in the mantle source approximates to the concentration of the subduction component relative to the total composition of the wedge. The approximation is because differences in partial melting between the MORB array and any arc array have a small influence on the equation.

$$X_{Ba}^{sz} = \frac{\left(\frac{Ba}{Yb}\right)_o - \left(\frac{Ba}{Yb}\right)_e}{\left(\frac{Ba}{Yb}\right)_o} \quad \text{(A6)}$$

[76] Note that this calculation gives the relative contributions to the mantle wedge. To calculate the

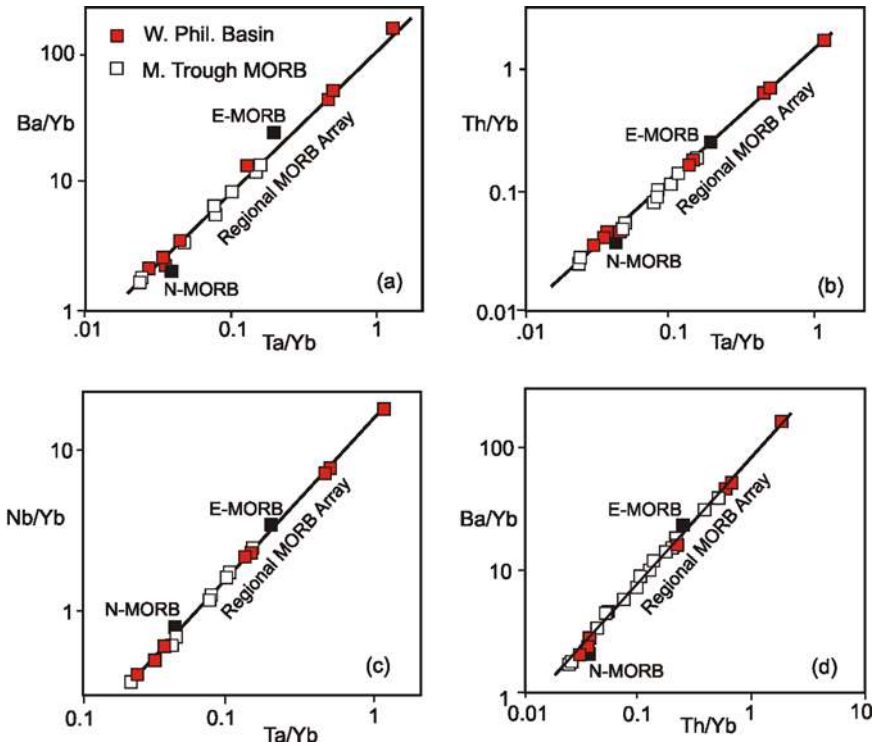

Figure A1. Definition of the MORB array using Eocene MORB and OIB lavas from DSDP Legs 31 and 59 in the West Philippine Basin together with Mariana Trough glasses with no apparent subduction component. Deviations from these MORB arrays on plots of M_1/Yb versus M_2/Yb then refer to the percentage of subduction-derived element M_1 in the mantle source, assuming that M_2 is subduction-immobile (= $\Delta M_1 - M_2$). The average N-MORB and E-MORB values of *Sun and McDonough* [1989] are represented as black squares. Note that the regional MORB array has higher Ba/Yb than the N-MORB average, reflecting its Indian MORB, rather than Pacific MORB, characteristics.

absolute additions to the mantle wedge (element fluxes), it is necessary to know more about the petrogenesis. This is much more complicated and will be attempted in a separate paper.

[77] The result is that the percentage of the added element can be contoured as lines parallel to the mantle array, as shown on Figure 6. The minimum value at which the component can be detected is defined as $2\sigma_M/M_o$ where $2\sigma_M$ is the 2-sigma error for element M on the MORB array, typically about 15%.

Appendix B: Correction for the Nb-Th-Ba Component

[78] The displacement of Mariana arc NSP samples, and a small number of basin and other arc samples, from the MORB array on the Nb-Ta diagram is unusual but demonstrates the presence of a component containing Nb and Ta. This component is described in the text as a Nb-Th-Ba component as it contains all three of these elements. This means that the component must be subtracted in order to determine the compositions and distributions of the components containing no Ta or Nb. This subtraction is not simple because processes other than mixing are involved. We therefore apply an empirical correction here.

[79] The key to this correction is the ratio of Nb to Ta in the high-Nb component. The Nb:Ta vector formed by samples with variable Nb-Th-Ba component has a gradient which approximates to 2:1 compared to a gradient of 1.05:1 formed by normal MORB processes (see Figure 7d). The aim is then to project back along the component addition vector until the MORB line is reached.

[80] Figure B1a demonstrates how this can be done. Take $(Nb/Yb)_o$ as the observed ratio in the lava, $(Nb/Yb)_e$ as the expected ratio calculated by assuming Ta is immobile, and $(Nb/Yb)_{e'}$ as the expected ratio represented by the intersection of the subduction addition vector and the MORB array. Take the slope of the MORB array as m and the slope of the subduction addition vector as M. Then

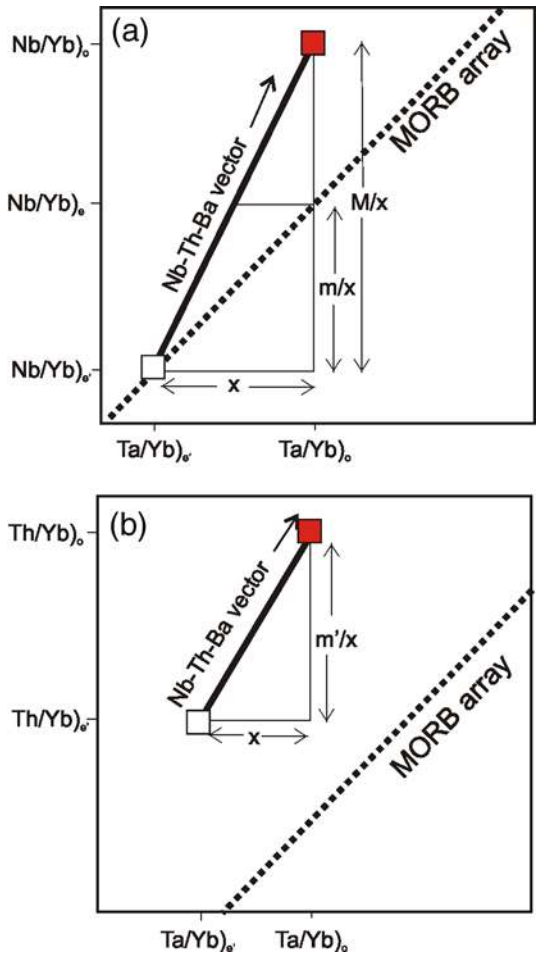

Figure B1. Diagrams illustrating the method of subtracting the Nb-Th-Ba component for (a) the Nb/Yb-Ta/Yb diagram and (b) the Th/Yb-Ta/Yb diagram. In each case, the red square gives the composition before subtraction and the open square gives the composition after subtraction. If the slopes of the MORB array and Nb-Th-Ba and Th-Ba component trends are known, or can be estimated, then equations may be written for the component subtraction.

the geometry of the diagram (similar triangles) shows that

$$\frac{\log\left(\frac{Nb}{Yb}\right)_o - \log\left(\frac{Nb}{Yb}\right)_{e'}}{\log\left(\frac{Nb}{Yb}\right)_e - \log\left(\frac{Nb}{Yb}\right)_{e'}} = \frac{M}{m},$$

from which

$$m\log\left(\frac{Nb}{Yb}\right)_o - m\log\left(\frac{Nb}{Yb}\right)_{e'} = M\log\left(\frac{Nb}{Yb}\right)_e - M\log\left(\frac{Nb}{Yb}\right)_{e'},$$

$$(M-m)\log\left(\frac{Nb}{Yb}\right)_{e'} = M\log\left(\frac{Nb}{Yb}\right)_e - m\log\left(\frac{Nb}{Yb}\right)_o,$$

$$\log\left(\frac{Nb}{Yb}\right)_{e'} = \frac{M}{M-m}\log\left(\frac{Nb}{Yb}\right)_e - \frac{m}{M-m}\log\left(\frac{Nb}{Yb}\right)_o,$$

$$\left(\frac{Nb}{Yb}\right)_{e'} = \frac{\left(\frac{Nb}{Yb}\right)_e^{\left(\frac{M}{M-m}\right)}}{\left(\frac{Nb}{Yb}\right)_o^{\left(\frac{m}{M-m}\right)}}, \quad \text{(B1)}$$

where $(Nb/Yb)_e$ is calculated from equation (A3).

[81] The percentage of added Nb in the mantle is then, as then given by

$$X_{Nb}^{\text{added}} = \frac{\left(\frac{Nb}{Yb}\right)_o - \left(\frac{Nb}{Yb}\right)_{e'}}{\left(\frac{Nb}{Yb}\right)_o}, \quad \text{(B2)}$$

and the Ta/Yb ratio prior to addition of the Nb-Th-Ba component is (again from equation (A3))

$$\left(\frac{Ta}{Yb}\right)_{e'} = 10^{\left(0.95\log(Nb/Yb)_{e'} - 1.17\right)}. \quad \text{(B3)}$$

[82] Th may then be corrected by projecting back along the component addition vector until the recalculated Ta/Yb ratio is reached, as shown in Figure B1b. The new Th/Yb ratios will then represent the values prior to addition of the Nb-Th-Ba component.

$$\left(\frac{Th}{Yb}\right)_{e'} = \left(\frac{Th}{Yb}\right)_o \left(\frac{\left(\frac{Ta}{Yb}\right)_{e'}}{\left(\frac{Ta}{Yb}\right)_o}\right)^{m'}, \quad \text{(B4)}$$

where $(Th/Yb)_{e'}$ and $(Ta/Yb)_{e'}$ is the ratio after correction, $(Th/Yb)_o$ and $(Ta/Yb)_o$ are the observed ratio, and m' is the slope of the Nb-Th-Ba component addition vector in Figure B1b (=3.5).

[83] Ba cannot be corrected in the same way, because the effects of the Nb-Th-Ba component are masked by the later additions. Thus we have to utilize the information from Figure 7g that Ba and Th behave similarly in both the Nb-Th-Ba and Th-Ba components. The Ba correction can then be made from the Th correction in equation (B4),

where m′ is the slope of the Nb-Th-Ba vector on the Th-Ba diagram (=1.1)

$$\left(\frac{Ba}{Yb}\right)_{e'} = \left(\frac{Ba}{Yb}\right)_{o} \left(\frac{\left(\frac{Th}{Yb}\right)_{e'}}{\left(\frac{Th}{Yb}\right)_{o}} \right)^{m''} . \quad \text{(B5)}$$

Acknowledgments

[84] Sample collection was partially supported by NSF grant OCE-0001827 to R.J.S. and NSF grants OCE9907063 and OCE0002584 to P.F. Geochemical analyses were supported by a Joint Infrastructure grant (NER/H/S/2000/00862) to J.A.P. and aided by advice from Iain McDonald. We thank Tim Elliott, Jim Gill, and Yoshiyuki Tatsumi for their constructive reviews. This is a contribution to the US MARGINS program.

References

Ayers, J. C., and E. B. Watson (1993), Rutile solubility and mobility in supercritical aqueous fluids, *Contrib. Mineral. Petrol.*, *114*, 321–330.

Bloomer, S. H., R. J. Stern, and N. C. Smoot (1989a), Physical volcanology of the submarine Mariana and Volcano Arcs, *Bull. Volcanol.*, *51*, 210–224.

Bloomer, S. H., R. J. Stern, E. Fisk, and C. H. Geschwind (1989b), Shoshonitic volcanism in the Northern Mariana Arc: 1. Mineralogic and major and trace element characteristics, *J. Geophys. Res.*, *94*, 4469–4496.

Breeding, C. M., J. J. Ague, and M. Bröcker (2004), Fluid-metasedimentary rock interactions in subduction-zone mélange: Implications for the chemical composition of arc magmas, *Geology*, *32*, 1041–1044.

Brenan, J. M., H. F. Shaw, D. L. Phinney, and F. J. Ryerson (1994), Rutile aqueous fluid partitioning of Nb, Ta, Hf, Zr, U and Th: Implications for high field strength element depletions in island arc basalts, *Earth Planet. Sci. Lett.*, *128*, 327–339.

Clift, P. D., and J. Lee (1998), Temporal evolution of the Mariana arc during rifting of the Mariana Trough traced through the volcaniclastic record, *Island Arc*, *7*, 496–512.

Dixon, T. H., and R. J. Stern (1983), Petrology, chemistry, and isotopic composition of submarine volcanoes in the southern Mariana arc, *Geol. Soc. Am., Bull.*, *94*, 1159–1172.

Eggins, S. M., J. D. Woodhead, L. P. J. Kinsley, G. E. Mortimer, P. Sylvester, M. T. McCulloch, J. M. Hergt, and M. R. Handler (1997), A simple method for the precise determination of ≤40 trace elements in geological samples by ICPMS using enriched isotope internal standardisation, *Chem. Geol.*, *134*, 311–326.

Eiler, J. M., A. Crawford, T. Elliott, K. A. Farley, J. W. Valley, and E. M. Stolper (2000), Oxygen isotope geochemistry of oceanic-arc lavas, *J. Petrol.*, *41*, 229–256.

Elliott, T., T. Plank, A. Zindler, W. White, and B. Bourdon (1997), Element transport from slab to volcanic front at the Mariana arc, *J. Geophys. Res.*, *102*, 14,991–15,019.

Fryer, P. (1995), Geology of the Mariana Trough, in *Back-Arc Basins*: *Tectonics and Magmatism*, edited by B. Taylor, pp. 237–279, Springer, New York.

Fryer, P., J. B. Gill, and M. C. Jackson (1997), Volcanologic and tectonic evolution of the Kasuga seamounts, northern Mariana Trough: Alvin submersible investigations, *J. Volcanol. Geotherm. Res.*, *79*, 277–311.

Fryer, P., H. Fujimoto, M. Sekine, L. E. Johnson, J. Kasahara, H. Masuda, T. Gamo, T. Ishii, M. Ariyoshi, and K. Fujiyoka (1998), Volcanoes of the southwestern extension of the active Mariana island arc: New swath-mapping and geochemical studies, *Island Arc*, *7*, 596–607.

Green, T. H. (1995), Significance of Nb/Ta as an indicator of geochemical processes in the crust-mantle system, *Chem. Geol.*, *120*, 347–359.

Gribble, R. F., R. J. Stern, S. H. Bloomer, D. Stüben, T. O'Hearn, and S. Newman (1996), MORB mantle and subduction components interact to generate basalts in the southern Mariana Trough back-arc basin, *Geochim. Cosmochim. Acta*, *60*, 2153–2166.

Gribble, R. F., R. J. Stern, S. Newman, S. H. Bloomer, and T. O'Hearn (1998), Chemical and isotopic composition of lavas from the northern Mariana Trough: Implications for magmagenesis in back-arc basins, *J. Petrol.*, *39*, 125–154.

Hawkins, J. W., P. F. Lonsdale, J. D. Macdougall, and A. M. Volpe (1990), Petrology of the axial ridge of the Mariana Trough backarc spreading center, *Earth Planet. Sci. Lett.*, *100*, 226–250.

Hoernle, K., G. Tilton, M. J. Le Bas, S. Duggen, and D. Garbe-Schönberg (2002), Geochemistry of oceanic carbonatites compared with continental carbonatites: Mantle recycling of oceanic crustal carbonate, *Contrib. Mineral. Petrol.*, *142*, 520–542.

Hussong, D. M., and P. Fryer (1983), Back-arc seamounts and the Sea-MARC II seafloor mapping system, *Eos Trans AGU*, *64*, 627–632.

Ikeda, Y., K. Nagao, R. J. Stern, M. Yuasa, and S. Newman (1998), Noble gases in pillow basalt glasses from the northern Mariana Trough back-arc basin, *Island Arc*, *7*, 471–478.

Ito, E., and R. J. Stern (1985), Oxygen and strontium-isotopic investigations of subduction zone volcanism: The case of the Volcano Arc and the Mariana island arc, *Earth Planet. Sci. Lett.*, *76*, 312–320.

Ito, E., R. J. Stern, and C. Douthitt (2003), Insights into operation of the "Subduction Factory" from the oxygen isotopic values of Southern Izu-Bonin-Mariana arc, *Island Arc*, *12*, 383–397.

Johnson, M. C., and T. Plank (1999), Dehydration and melting experiments constrain the fate of subducted sediments, *Geochem. Geophys. Geosyst.*, *1*(1), doi:10.1029/1999GC000014.

Kato, T., J. Beavan, T. Matsushima, Y. Kotake, J. T. Camacho, and S. Nakao (2003), Geodetic evidence of back-arc spreading in the Mariana Trough, *Geophys. Res. Lett.*, *30*(12), 1625, doi:10.1029/2002GL016757.

Kay, S. M., and J. M. Abbrazzi (1996), Magmatic evidence for Neogene lithospheric evolution of the central Andean "flat slab" between 30° and 32°S, *Tectonophysics*, *259*, 15–28.

Keppler, H. (1996), Constraints from partitioning experiments on the composition of subduction-zone fluids, *Nature*, *380*, 237–240.

Lin, P. N., R. J. Stern, and S. H. Bloomer (1989), Shoshonitic volcanism in the Northern Mariana Arc: 2. Large-ion lithophile and rare earth element abundances: Evidence for the source of incompatible element enrichments in intraoceanic arcs, *J. Geophys. Res.*, *94*, 4497–4514.

MacPherson, C. G., and R. Hall (2001), Tectonic setting of Eocene boninite magmatism in the Izu-Bonin-Mariana forearc, *Earth Planet. Sci. Lett.*, *186*, 215–230.

Martinez, F., and B. Taylor (2002), Mantle wedge control on back-arc accretion, *Nature*, *416*, 417–420.

Martinez, F., P. Fryer, N. A. Baker, and T. Yamazaki (1995), Evolution of backarc rifting: Mariana Trough, 20°–24°N, *J. Geophys. Res.*, *100*, 3807–3827.

Martinez, F., P. Fryer, and N. Becker (2000), Geophysical characteristics of the southern Mariana Trough, 11°50′N-13°40′N, *J. Geophys. Res.*, *105*, 16,591–16,607.

McCulloch, M. T., and A. J. Gamble (1991), Geochemical and geodynamical constraints on subduction zone magmatism, *Earth Planet. Sci. Lett.*, *102*, 358–374.

Münker, C., G. Wörner, G. Yogodzinski, and T. Churikova (2004), Behaviour of high field strength elements in subduction zones: Constraints from Kamchatka-Aleutian arc lavas, *Earth Planet. Sci. Lett.*, *224*, 275–293.

Pearce, J. A., P. E. Baker, P. K. Harvey, and I. W. Luff (1995), Geochemical evidence for subduction fluxes, mantle melting and fractional crystallization beneath the South Sandwich island arc, *J. Petrol.*, *36*, 1073–1109.

Pearce, J. A., P. D. Kempton, G. M. Nowell, and S. R. Noble (1999), Hf-Nd element and isotope perspective on the nature and provenance of mantle and subduction components in Western Pacific arc-basin systems, *J. Petrol.*, *40*, 1579–1611.

Peate, D. W., and J. A. Pearce (1998), Causes of spatial compositional variations in Mariana arc lavas: Trace element evidence, *Island Arc*, *7*, 479–495.

Ryerson, F. J., and E. B. Watson (1987), Rutile saturation in magmas: Implications for Ti-Nb-Ta depletion in island arc basalts, *Earth Planet. Sci. Lett.*, *86*, 225–239.

Sinton, J. H., and P. Fryer (1987), Mariana Trough lavas from 18°N: Implications for the origin of back arc basin basalts, *J. Geophys. Res.*, *92*, 12,782–12,802.

Sorensen, S. S., and J. N. Grossman (1989), Enrichment of trace elements in garnet amphibolites from a palaeo-subduction zone: Catalina Schist, Southern California, *Geochim. Cosmochim. Acta*, *53*, 3155–3177.

Stern, R. J., and L. D. Bibee (1984), Esmeralda Bank: Geochemistry of an active submarine volcano in the Mariana Island Arc, *Contrib. Mineral. Petrol.*, *86*, 159–169.

Stern, R. J., S. H. Bloomer, P.-N. Lin, E. Ito, and J. Morris (1988), Shoshonitic magmas in nascent arcs: New evidence from submarine volcanoes in the northern Marianas, *Geology*, *16*, 426–430.

Stern, R. J., S. H. Bloomer, P.-N. Lin, and N. C. Smoot (1989), Submarine arc volcanism in the southern Mariana Arc as an ophiolite analogue, *Tectonophysics*, *168*, 151–170.

Stern, R. J., P.-N. Lin, J. D. Morris, M. C. Jackson, P. Fryer, S. H. Bloomer, and E. Ito (1990), Enriched back-arc basin basalts from the northern Mariana Trough: Implications for the magmatic evolution of back-arc basins, *Earth Planet. Sci. Lett.*, *100*, 210–225.

Stern, R. J., M. C. Jackson, P. Fryer, and E. Ito (1993), Sr, Nd and Pb isotopic composition of the Kasuga cross-chain in the Mariana Arc: A new perspective on the K-*h* relationship, *Earth Planet. Sci. Lett.*, *119*, 459–475.

Stern, R. J., M. J. Fouch, and S. L. Klemperer (2003), An overview of the Izu-Bonin-Mariana subduction factory, in *Inside the Subduction Factory*, *Geophys. Monogr. Ser.*, vol. 138, edited by J. Eiler, pp. 175–222, AGU, Washington, D. C.

Stolper, E., and S. Newman (1994), The role of water in the petrogenesis of Mariana Trough magmas, *Earth Planet. Sci. Lett.*, *121*, 293–325.

Stüben, D., T. Neumann, N. E. Taibi, and G. P. Glasby (1998), Segmentation of the southern Mariana back-arc spreading center, *Island Arc*, *7*, 513–524.

Sun, C. H., and R. J. Stern (2001), Genesis of Mariana shoshonites: Contribution of the subduction component, *J. Geophys. Res.*, *106*, 589–608.

Sun, S.-S., and W. F. McDonough (1989), Chemical and isotopic systematics of oceanic basalts: Implications for mantle composition and processes, *Geol. Soc. Spec. Publ.*, *42*, 313–345.

Taylor, B., and F. Martinez (2003), Back-arc basin basalt systematics, *Earth Planet. Sci. Lett.*, *210*, 481–497.

Volpe, A. M., J. D. Macdougall, and J. W. Hawkins (1987), Mariana Trough basalts (MTB): Trace element and Sr-Nd isotopic evidence for mixing between MORB-like and arc-like melts, *Earth Planet. Sci. Lett.*, *82*, 241–254.

Woodhead, J. D. (1989), Geochemistry of the Mariana arc (western Pacific): Source compositions and processes, *Chem. Geol.*, *76*, 1–24.

Woodhead, J., S. Eggins, and J. Gamble (1993), High field strength and transition element systematics in island arc and back-arc basin basalts: Evidence for multi-phase melt extraction and a depleted mantle wedge, *Earth Planet. Sci. Lett.*, *114*, 491–504.

Woodhead, J. D., J. M. Hergt, J. P. Davidson, and S. M. Eggins (2001), Hafnium isotope evidence for "conservative" element mobility during subduction zone processes, *Earth Planet. Sci. Lett.*, *192*, 331–346.

Yamazaki, T., N. Seama, K. Okino, K. Kitada, M. Joshima, H. Oda, and J. Naka (2003), Spreading process of the northern Mariana Trough: Rifting-spreading transition at 22°N, *Geochem. Geophys. Geosyst.*, *4*(9), 1075, doi:10.1029/2002GC000492.